

CONDENSATION HEAT TRANSFER
INSIDE
ROTATING HEAT PIPES

Chaiyuth Tantrakul

DUDLEY KNOX LIBRARY
NAVAL POSTGRADUATE SCHOOL
MONTEREY, CALIFORNIA 93943-5002

NAVAL POSTGRADUATE SCHOOL

Monterey, California



THESIS

CONDENSATION HEAT TRANSFER
INSIDE
ROTATING HEAT PIPES

by

Chaiyuth Tantrakul

June 1977

Thesis Advisor:

P. J. Marto

Approved for public release; distribution unlimited.

T179599

REPORT DOCUMENTATION PAGE		READ INSTRUCTIONS BEFORE COMPLETING FORM
1. REPORT NUMBER	2. GOVT ACCESSION NO.	3. RECIPIENT'S CATALOG NUMBER
4. TITLE (and Subtitle) Condensation Heat Transfer Inside Rotating Heat Pipes		5. TYPE OF REPORT & PERIOD COVERED Master's and Engineer's Thesis; June 1977
		6. PERFORMING ORG. REPORT NUMBER
7. AUTHOR(s) Chaiyuth Tantrakul		8. CONTRACT OR GRANT NUMBER(s)
9. PERFORMING ORGANIZATION NAME AND ADDRESS Naval Postgraduate School Monterey, California 93940		10. PROGRAM ELEMENT, PROJECT, TASK AREA & WORK UNIT NUMBERS
11. CONTROLLING OFFICE NAME AND ADDRESS Naval Postgraduate School Monterey, California 93940		12. REPORT DATE June 1977
		13. NUMBER OF PAGES 103
14. MONITORING AGENCY NAME & ADDRESS (If different from Controlling Office)		15. SECURITY CLASS. (of this report) Unclassified
		15a. DECLASSIFICATION/DOWNGRADING SCHEDULE
16. DISTRIBUTION STATEMENT (of this Report) Approved for public release; distribution unlimited.		
17. DISTRIBUTION STATEMENT (of the abstract entered in Block 20, if different from Report)		
18. SUPPLEMENTARY NOTES		
19. KEY WORDS (Continue on reverse side if necessary and identify by block number) Condensation Heat Transfer		
20. ABSTRACT (Continue on reverse side if necessary and identify by block number) An analytical study was undertaken to determine two-dimensional wall conduction effects during film condensation on an internally finned, rotating heat pipe. An earlier Finite Element method was modified to solve the problem by using different numbers of axial increments and different numbers of elements. Resulting heat transfer rates were shown to be similar to those obtained earlier.		

(20. ABSTRACT Continued)

A rotating heat pipe was tested using various copper condensers including two smooth-wall cylinders and a 0.5 degree truncated cone. All condensers were tested at different rotational speeds using distilled water as the working fluid. In the case of the 1.46 inch diameter cylindrical condenser, data were also taken with Freon 113 and ethanol. The heat transfer rate of each condenser was plotted against the saturation temperature of the vapor.

Using the experimental results obtained in this thesis, together with the data of earlier theses, a comparison was made with the theoretical analysis of Roetzel. Agreement is reasonable, and Roetzel's analysis can be used to predict overall rotating heat pipe performance to within ± 20 percent for water. The data for Freon 113 and ethanol, however, fall approximately 35 percent higher than this theory.

Condensation Heat Transfer
Inside
Rotating Heat Pipes

by

Chaiyuth Tantrakul
Lieutenant, Royal Thai Navy
B.S., Royal Thai Naval Academy, 1967

Submitted in partial fulfillment of the
requirements for the degrees of

MASTER OF SCIENCE IN MECHANICAL ENGINEERING

and

MECHANICAL ENGINEER

from the

NAVAL POSTGRADUATE SCHOOL
June 1977

ABSTRACT

An analytical study was undertaken to determine two-dimensional wall conduction effects during film condensation on an internally finned, rotating heat pipe. An earlier Finite Element method was modified to solve the problem by using different numbers of axial increments and different numbers of elements. Resulting heat transfer rates were shown to be similar to those obtained earlier.

A rotating heat pipe was tested using various copper condensers including two smooth-wall cylinders and a 0.5 degree truncated cone. All condensers were tested at different rotational speeds using distilled water as the working fluid. In the case of the 1.46 inch diameter cylindrical condenser, data were also taken with Freon 113 and ethanol. The heat transfer rate of each condenser was plotted against the saturation temperature of the vapor.

Using the experimental results obtained in this thesis, together with the data of earlier theses, a comparison was made with the theoretical analysis of Roetzel. Agreement is reasonable, and Roetzel's analysis can be used to predict overall rotating heat pipe performance to within ± 20 percent for water. The data for Freon 113 and ethanol, however, fall approximately 35 percent higher than this theory.

TABLE OF CONTENTS

I.	INTRODUCTION -----	13
A.	THE ROTATING HEAT PIPE -----	13
B.	ROTATING HEAT PIPE LIMITATIONS -----	13
1.	Sonic Limit -----	15
2.	Boiling Limit -----	17
3.	Entrainment Limit -----	19
4.	Condensing Limit -----	20
C.	THEORETICAL INVESTIGATIONS OF FILM CONDENSATION ON SMOOTH ROTATING CONDENSER SURFACES -----	21
D.	ANALYSIS OF FINNED ROTATING CONDENSER SURFACES -----	38
E.	THESIS OBJECTIVES -----	41
II.	FINITE ELEMENT ANALYSIS AND RESULTS -----	43
A.	REVIEW OF EARLIER ANALYSES -----	43
B.	MODIFICATION TO THE FINITE ELEMENT ANALYSIS -----	52
C.	DISCUSSION OF NUMERICAL RESULTS -----	63
III.	EXPERIMENTAL PROGRAM -----	66
A.	EXPERIMENTAL EQUIPMENT -----	66
1.	Description of Equipment -----	66
2.	Instrumentation -----	70
B.	EXPERIMENTAL PROCEDURES -----	73
1.	Preparation of Condenser Wall -----	73
2.	Filling and Venting Procedures -----	74

3.	Run Procedures -----	75
4.	Data Reduction -----	76
IV.	DISCUSSION OF EXPERIMENTAL RESULTS -----	78
A.	EXPERIMENTAL RESULTS -----	78
B.	ANALYSIS OF THE RESULTS -----	83
V.	CONCLUSIONS AND RECOMMENDATIONS -----	94
A.	CONCLUSIONS -----	94
B.	RECOMMENDATIONS -----	94
APPENDIX A:	CALIBRATION OF MEASUREMENT DEVICES ---	96
APPENDIX B:	UNCERTAINTY ANALYSIS -----	98
BIBLIOGRAPHY	-----	101
INITIAL DISTRIBUTION LIST	-----	103

LIST OF TABLES

1.	Specifications of a Typical Rotating Heat Pipe -----	15
2.	Theoretical Finned Condenser Heat Transfer Rate Versus Number of Axial Increments, $h_{out} = 1000 \text{ BTU/hr-ft}^2\text{-deg F}$ -----	53
3.	Theoretical Finned Condenser Heat Transfer Rate Versus Number of Axial Increments, $h_{out} = 1500 \text{ BTU/hr-ft}^2\text{-deg F}$ -----	54
4.	Theoretical Finned Condenser Heat Transfer Rate Versus Number of Axial Increments, $h_{out} = 5000 \text{ BTU/hr-ft}^2\text{-deg F}$ -----	55
5.	Comparison of Theoretical Finned Condenser Heat Transfer Rates at 1000 RPM, for $h_{out} = 1000 \text{ BTU/hr-ft}^2\text{-deg F}$ -----	57
6.	Comparison of Theoretical Finned Condenser Heat Transfer Rates at 3000 RPM, for $h_{out} = 1000 \text{ BTU/hr-ft}^2\text{-deg F}$ -----	58
7.	Comparison of Theoretical Finned Condenser Heat Transfer Rates at 1000 RPM, for $h_{out} = 1500 \text{ BTU/hr-ft}^2\text{-deg F}$ -----	59
8.	Comparison of Theoretical Finned Condenser Heat Transfer Rates at 3000 RPM, for $h_{out} = 1500 \text{ BTU/hr-ft}^2\text{-deg F}$ -----	60
9.	Comparison of Theoretical Finned Condenser Heat Transfer Rates at 1000 RPM, for $h_{out} = 5000 \text{ BTU/hr-ft}^2\text{-deg F}$ -----	61
10.	Comparison of Theoretical Finned Condenser Heat Transfer Rates at 3000 RPM, for $h_{out} = 5000 \text{ BTU/hr-ft}^2\text{-deg F}$ -----	62
11.	Summary of Experimental Runs -----	79

LIST OF FIGURES

1.	Schematic Drawing of a Rotating Heat Pipe -----	14
2.	Operating Limits of a Typical, Water-filled Rotating Heat Pipe -----	18
3.	Coordinate System and Geometry for Laminar Film Condensation on a Rotating Truncated Cone -----	25
4.	Schematic Drawing of Paper Drying Drum with Two Curved Conical Sections and One Sampling Groove --	35
5.	Internally Finned Condenser Geometry Showing Fins, Troughs and Lines of Symmetry -----	39
6.	Condenser Geometry Considered in Analysis -----	40
7.	Alternate Condenser Wall Geometry -----	42
8.	Condenser Geometry Considered in Two-Dimensional Analysis with 2 Finite Elements -----	45
9.	Computer Program Flowchart of Two-Dimensional Conduction Analysis of Corley -----	49
10.	Condenser Geometry Considered in Two-Dimensional Analysis with 3 Finite Elements -----	56
11.	Condenser Geometry Considered in Two-Dimensional Analysis with 4 Finite Elements -----	64
12.	Cross Section of the Rotating Heat Pipe -----	67
13.	Schematic Diagram of Heat Pipe Apparatus -----	68
14.	Impingement Cooling Schematic -----	69
15.	Thermocouple Positions for 1.46 Inch Diameter and 1.00 Inch Diameter Cylinder -----	71
16.	Thermocouple Positions for 0.5 Degree Cone -----	72
17.	Heat Transfer Rate versus Saturation Temperature for Cylindrical 1.00 Inch Diameter Condenser -----	80
18.	Heat Transfer Rate versus Saturation Temperature for Cylindrical 1.46 Inch Diameter Condenser -----	81

19.	Heat Transfer Rate Versus Saturation Temperature for Truncated Cone Condenser With 0.5 Degree Half Angle -----	82
20.	Condenser Outside Surface Temperature Profile at 700 RPM for 1.46 Inch Diameter Cylindrical Condenser -----	84
21.	Condenser Outside Surface Temperature Profile at 1400 RPM for 1.46 Inch Diameter Cylindrical Condenser -----	85
22.	Condenser Outside Surface Temperature Profile at 2800 RPM for 1.46 Inch Diameter Cylindrical Condenser -----	86
23.	Condenser Outside Surface Temperature Profile at 700 RPM for 0.5 Degree Truncated Cone -----	87
24.	Nusselt Number Versus Sherwood Number for Cylindrical Condensers -----	90
25.	Nusselt Number Versus Sherwood Number for Truncated Cone Condensers -----	91
26.	Comparison of Experimental Data with Theory of Roetzel -----	93

TABLE OF SYMBOLS

A	cross sectional area for flow, ft^2
b	height of triangular grooves, ft
C_p	specific heat, BTU/lbm - deg F
f	friction factor, dimensionless
h	local condensation heat transfer coefficient, BTU/hr-ft ² -deg F
h_m	mean condensation heat transfer coefficient, BTU/hr-ft ² -deg F
h_{out}	coolant heat transfer coefficient, BTU/hr-ft ² -deg F
h_{fg}	latent heat of vaporization, BTU/lbm
k_f	thermal conductivity of condensate film, BTU/hr-ft-deg F
k_w	thermal conductivity of condenser wall, BTU/hr-ft-deg F
\dot{m}	mass flow rate of coolant, lbm/hr
\dot{M}_1	mass flow rate of vapor condensing on fin, lbm/hr
\dot{M}_2	mass flow rate of vapor condensing in trough, lbm/hr
\dot{M}_{total}	total mass flow rate of condensate, lbm/hr
P_v	pressure of the vapor, lbf/ft ²
\dot{Q}	theoretical heat transfer rate out of heat pipe, BTU/hr
R	internal radius of condenser, ft
R_o	minimum internal radius of condenser, ft
T_s	vapor saturation temperature, deg F
T_w	inside wall temperature, deg F
t	condenser wall thickness, ft

u	velocity of liquid in x direction, ft/sec
v	velocity of vapor, ft/sec
W_{cp}	uncertainty of specific heat, BTU/lbm-deg F
W_m	uncertainty of coolant mass flow rate, lbm/hr
$W_{\Delta T}$	uncertainty of coolant temperature difference, deg F
x	coordinate measuring distance along condenser length
y	coordinate measuring distance vertically from fin surface
z	coordinate measuring distance along fin surface

GREEK

α	fin half angle, degrees
δ	condensate film thickness, ft
δ^*	condensate film thickness in trough, ft
ϵ	local trough width, ft
ϵ_o	minimum width of trough, ft
ϕ	condenser half cone angle, degrees
ρ_f	density of the liquid, lbm/ft ³
ρ_v	density of the vapor, lbm/ft ³
σ	surface tension of the liquid, lbf/ft
τ	shear stress, lbf/ft ²
μ_f	viscosity of the liquid, lbm/ft-sec
μ_v	viscosity of the vapor, lbm/ft-sec
ω	angular velocity, rad/sec

ACKNOWLEDGMENTS

The author would like to express his sincere appreciation to Dr. P. J. Marto of the Naval Postgraduate School for his guidance, advice, and encouragement throughout the course of this thesis work.

I. INTRODUCTION

A. THE ROTATING HEAT PIPE

The rotating heat pipe is a closed rotating container capable of transferring large amounts of heat from rotating machinery. It consists of three main parts: (1) a cylindrical evaporator, (2) a cylindrical or truncated-cone condenser and (3) a working fluid. The operation of a rotating heat pipe is shown schematically in Figure 1.

When the rotating heat pipe is rotated above a critical speed, the working fluid forms an annulus in the evaporator. Heat input to the evaporator causes some of the working fluid to vaporize, and this vapor flows into the condenser transporting latent heat of vaporization. External cooling of the condenser allows the vapor to condense on the inner condenser wall. The centrifugal force due to the rotation has a component acting along the condenser wall which accelerates the condensate back to the evaporator.

B. ROTATING HEAT PIPE LIMITATIONS

Ballback [1] has studied the limitations imposed on the rotating heat pipe by various fluid dynamic mechanisms in a preliminary theoretical analysis of its operation. By using existing theories and experimental correlations, he was able to estimate the sonic limit, the boiling limit, the entrainment limit and the condensing limit of performance.

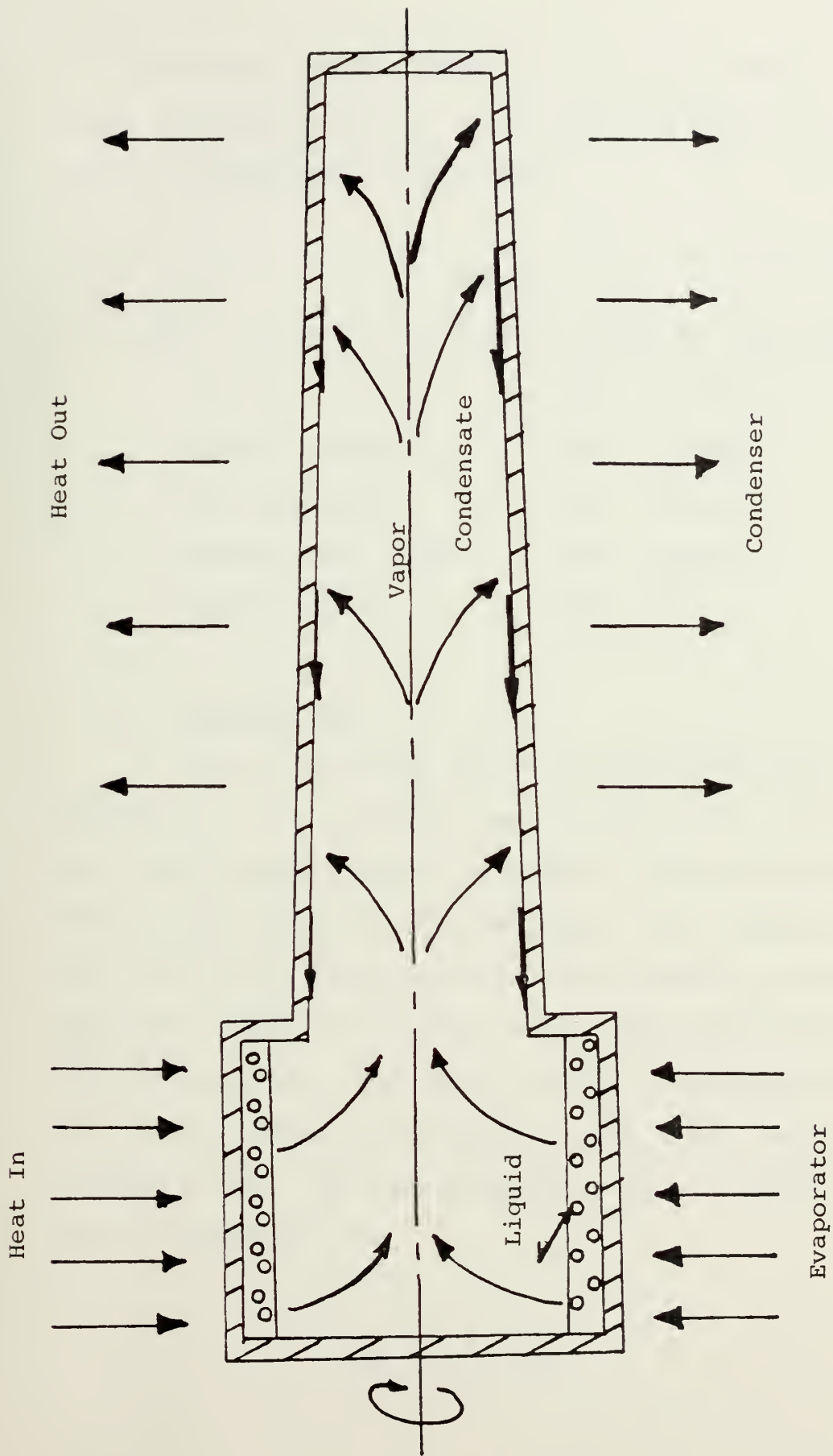


Figure 1. Schematic Drawing of a Rotating Heat Pipe

A typical rotating heat pipe with the physical dimensions as shown in Table 1 was chosen in order to demonstrate the predicted performance.

Table 1

Specifications of a Typical Rotating Heat Pipe

Length	14.000	inches
Minimum diameter	2.000	inches
Wall thickness	0.125	inches
Internal half angle	1.000	degree
Rotating speed	2700	RPM

1. Sonic Limit

As the heat flux in the rotating heat pipe is increased, it is possible that the flow rate of the vapor down the container may be limited by the attainment of a choked flow condition for the vapor. This choking of the vapor flow will definitely limit the amount of energy the vapor can transport down the pipe, thus limiting the operation of the pipe. The heat transfer mechanism employed in the rotating heat pipe depends on the latent energy of the working fluid. The heat transfer rate in the pipe may then be expressed as:

$$\dot{q}_t = \dot{m}_v h_{fg} \quad (1)$$

where

\dot{m}_v = mass flow rate of the vapor, lbm/hr.

From continuity, the mass flow rate of the vapor may be expressed by:

$$\dot{m}_v = \rho_v u_v A \quad (2)$$

where

u_v = velocity of the vapor, ft/sec

A = cross section area for the flow, ft².

Then

$$\dot{q}_t = \rho_v u_v A h_{fg} \quad (3)$$

The vapor velocity is taken as the sonic velocity, so that:

$$u_v = c = \sqrt{g_o kRT} \quad (4)$$

where

c = sonic velocity, ft/sec

g_o = acceleration of gravity, $32.1739 \frac{\text{ft-lbm}}{\text{lbf-sec}^2}$

k = the ratio of specific heats,

R = gas constant, ft-lbf/lbm-deg R

T = absolute temperature, deg R

Using equations (3) and (4), the sonic limit of a typical rotation heat pipe can be computed, as shown in Figure 2.

2. Boiling Limit

Kutateladze [2] has postulated that the transition from nucleate boiling to film boiling is purely a hydrodynamic phenomenon. Based on this assumption he has obtained the correlation formula for predicting the burnout heat flux:

$$\dot{q}_t = K \sqrt{\rho_v} A_b h_{fg} \{\sigma g [\rho_f - \rho_v]\}^{1/4} \quad (5)$$

where

A_b = heat transfer area in the boiler, ft^2

ρ_v = density of the vapor, lbm/ft^3

h_{fg} = latent heat of vaporization, BTU/lbm

σ = surface tension, lbf/ft

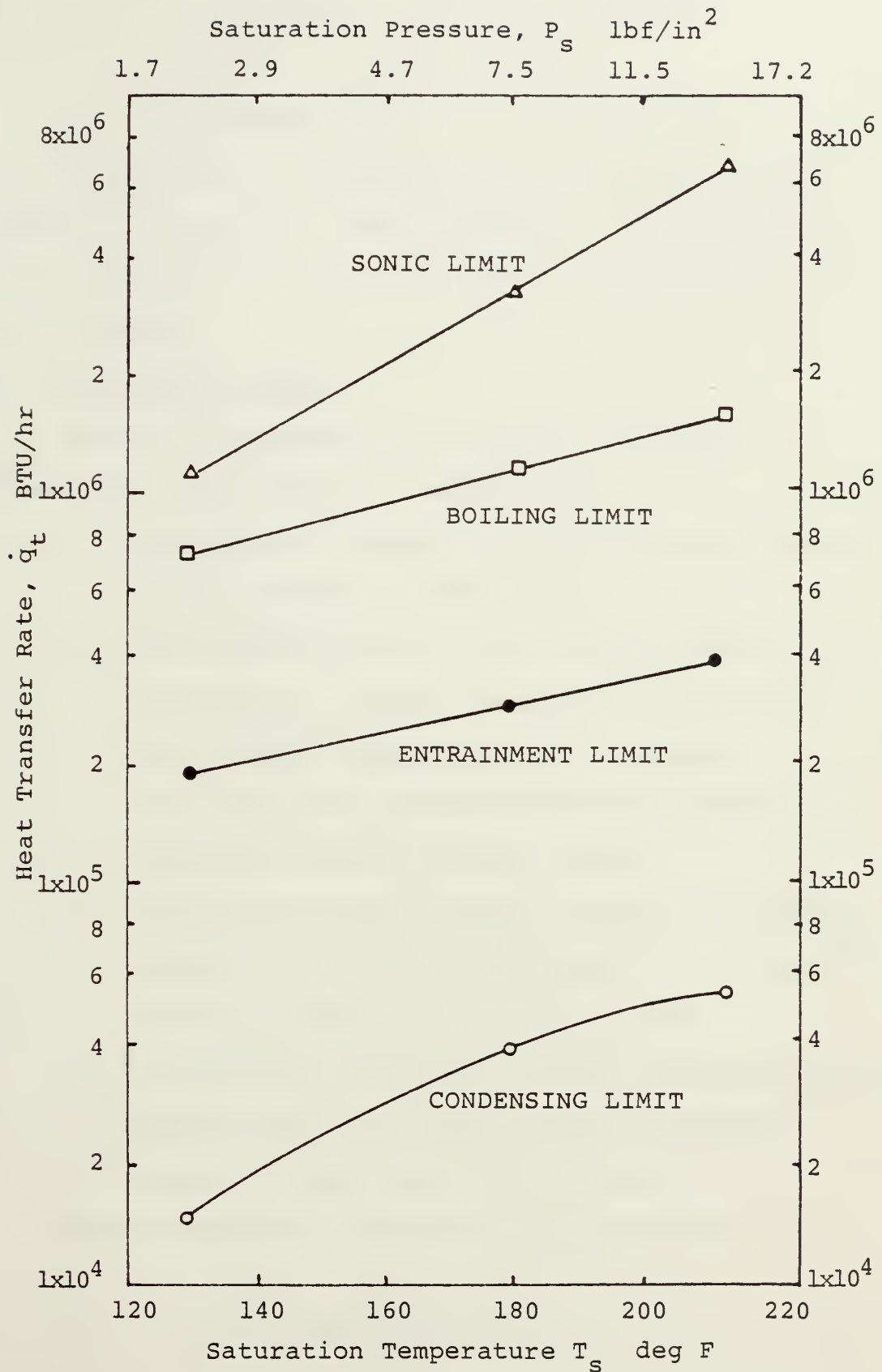


Figure 2. Operating Limits of a Typical, Water-Filled, Rotating Heat Pipe

g = acceleration of gravity, ft/hr²

ρ_f = density of fluid, lbm/ft³

K = constant value.

Kutateladze's experimental data indicate a value of K between 0.13 and 0.19. Using equation (5), the boiling limit of a typical rotating heat pipe can be computed, as shown in Figure 2.

3. Entrainment Limit

Sakhuja [3] studied the flooding constraint in wickless heat pipes, where he assumed that:

- a) the vapor and liquid are in counterflow motion and are exposed to each other;
- b) the falling film of liquid (under gravity) is subjected to a shear stress by counterflowing vapor, which tends to retard the film;
- c) the liquid film remains smooth and stable, and the shear stress is usually small;
- d) the buoyancy forces, due to density differences between the vapor and the liquid, are responsible for maintaining the counterflow; and
- e) the buoyancy forces are balanced with dissipative effects which are proportional to momentum fluxes of vapor and liquid streams.

He has obtained a correlation for flooding:

$$\dot{q}_t = \frac{A_x C^2 h_{fg} \sqrt{gD(\rho_f - \rho_v) \rho_v}}{[1 + (\rho_v/\rho_f)^{1/4}]^2} \quad (6)$$

where

- \dot{q}_t = heat transfer rate, BTU/hr
- A_x = flow area, ft²
- C = dimensionless constant, 0.725 for tube with sharp edged flange
- D = inside diameter of the heat pipe, ft
- g = acceleration due to gravity, ft/hr²
- ρ_f = density of the fluid, lbm/ft³
- ρ_v = density of the vapor, lbm/ft³
- h_{fg} = latent heat of vaporization, BTU/lbm.

Using equation (6), the entrainment limit of a typical rotating heat pipe can be computed and is shown in Figure 2.

4. Condensing Limit

The solution for condensation in the rotating heat pipe has been carried out by Ballback [1]. He modeled the condenser section of the heat pipe as a rotating, truncated cone, and an equation to compute the condensing limit was derived:

$$\dot{q}_t = \pi \left\{ \frac{2}{3} \frac{k_f^3 \rho_f^2 \omega^2 h_{fg} [T_s - T_w]^3}{\mu_f \sin^2 \phi} \right\}^{1/4} \{ [R_o + L \sin \phi]^{8/3} - R_o^{8/3} \}^{3/4} \quad (7)$$

where

- \dot{q}_t = total heat transfer rate, BTU/hr
- k_f = thermal conductivity of the condensate film, BTU/hr-ft-deg F

ρ_f	=	density of fluid, lbm/ft ³
ω	=	angular velocity, 1/hr
h_{fg}	=	latent heat of vaporization, BTU/lbm
T_s	=	saturation temperature, deg F
T_w	=	inside wall temperature, deg F
μ_f	=	viscosity of fluid, lbm/ft-hr
ϕ	=	half cone angle, degrees
R_o	=	minimum wall radius in the condenser section, ft
L	=	length along the wall of the condenser, ft.

Equation (7) is a function of the physical properties of the working fluid, the geometry of the rotating heat pipe and the operating speed. Using this equation, the condensing limit for a typical rotating heat pipe can be computed. This result is also shown in Figure 2.

It is clear from the results of Figure 2, that for the geometry and working fluid chosen, and under normal circumstances, the heat transfer rate is limited primarily by the amount of heat which can be transferred through the condenser wall. However, other limitations may become important as heat pipe geometry and operating conditions are altered.

C. THEORETICAL INVESTIGATIONS OF FILM CONDENSATION ON SMOOTH ROTATING CONDENSER SURFACES

Sparrow and Gregg [4] were the first to study condensation on a rotating surface. They studied condensation on a

rotating disk at uniform surface temperature, T_w , situated in a large quiescent body of pure saturated vapor. They assumed that the condensed liquid formed a continuous film on the disk and that fluid in this film moved radially outward along the disk under the action of the centrifugal force field. They arrived at the following solution for the situation where energy convection and acceleration terms are negligible:

$$\frac{h(\frac{v}{\omega})^{1/2}}{k_f} = 0.904 \left(\frac{Pr}{C_p \Delta T / h_{fg}} \right) \quad (8)$$

where

- h = local heat transfer coefficient, BTU/hr-ft²-deg F
- k_f = thermal conductivity of condensate, BTU/hr-ft-deg F
- v = kinematic viscosity of condensate, ft²/hr
- ω = angular velocity, 1/hr
- Pr = Prandtl number, $\mu C_p / k_f$
- μ = absolute viscosity of condensate, lbm/ft-hr
- C_p = specific heat of condensate, BTU/lbm-deg F
- T_w = disk surface temperature, deg F
- T_{sat} = saturation temperature of vapor, deg F
- ΔT = $T_{sat} - T_w$, deg F
- h_{fg} = latent heat of vaporization, BTU/lbm.

Equation (8) predicts that the local heat transfer coefficient is constant across the disk and does not vary with radial position.

Sparrow and Hartnett [5] continued the research using a rotating cone with the same assumptions used earlier. Their result for the heat transfer coefficient was:

$$h_{\text{cone}}/h_{\text{disk}} = (\sin \phi)^{1/2} \quad (9)$$

where ϕ is the internal half-angle of the cone. As pointed out by the authors, however, equation (9) applies only to cones that are not too slender. Using their result, the mean Nusselt number for a cone can be written as:

$$\text{Nu}_m = \frac{hL}{k} = 0.904 \left(\frac{\omega^2 \sin^2 \phi L^4}{\nu^2} \frac{\text{Pr}}{C_p \Delta T / h_{fg}} \right)^{1/4} \quad (10)$$

Leppert and Nimmo [6,7] studied laminar film condensation on a surface normal to body or inertial forces such as a finite horizontal surface, or a rotating drum. They found that the local heat transfer coefficient varies with position, and the mean Nusselt number, for a constant surface temperature, with negligible surface tension effects, is:

$$\text{Nu}_m = 0.64 \text{Sh}^{1/5} \quad (11)$$

where

$$\text{Nu}_m = \text{mean Nusselt number, } \frac{h_m L}{k}$$

$$\text{Sh} = \text{Sherwood number, } \frac{g \rho^2 h_{fg} L^3}{k \Delta T \mu} .$$

Equation (11) can be applied to the case of condensation on the inside of a rotating cylinder of radius, r , where g is replaced by $r\omega^2$.

The first theoretical investigation conducted at the Naval Postgraduate School was performed by Ballback [1]. His analysis was a Nusselt type analysis for film condensation on the inside surface of a rotating truncated cone of half angle cone, ϕ , with a geometry defined in Figure 3. His assumptions were similar to those used in the Nusselt analysis of film condensation on a vertical wall, namely:

- 1) steady state condition,
- 2) film condensation, not dropwise condensation,
- 3) laminar flow of condensate,
- 4) constant fluid properties,
- 5) no condensate subcooling,
- 6) no momentum change through the condensate,
- 7) no liquid-vapor interfacial shear stresses,
- 8) linear distribution of temperature through the condensate film,
- 9) negligible force of gravity, and
- 10) constant wall temperature.

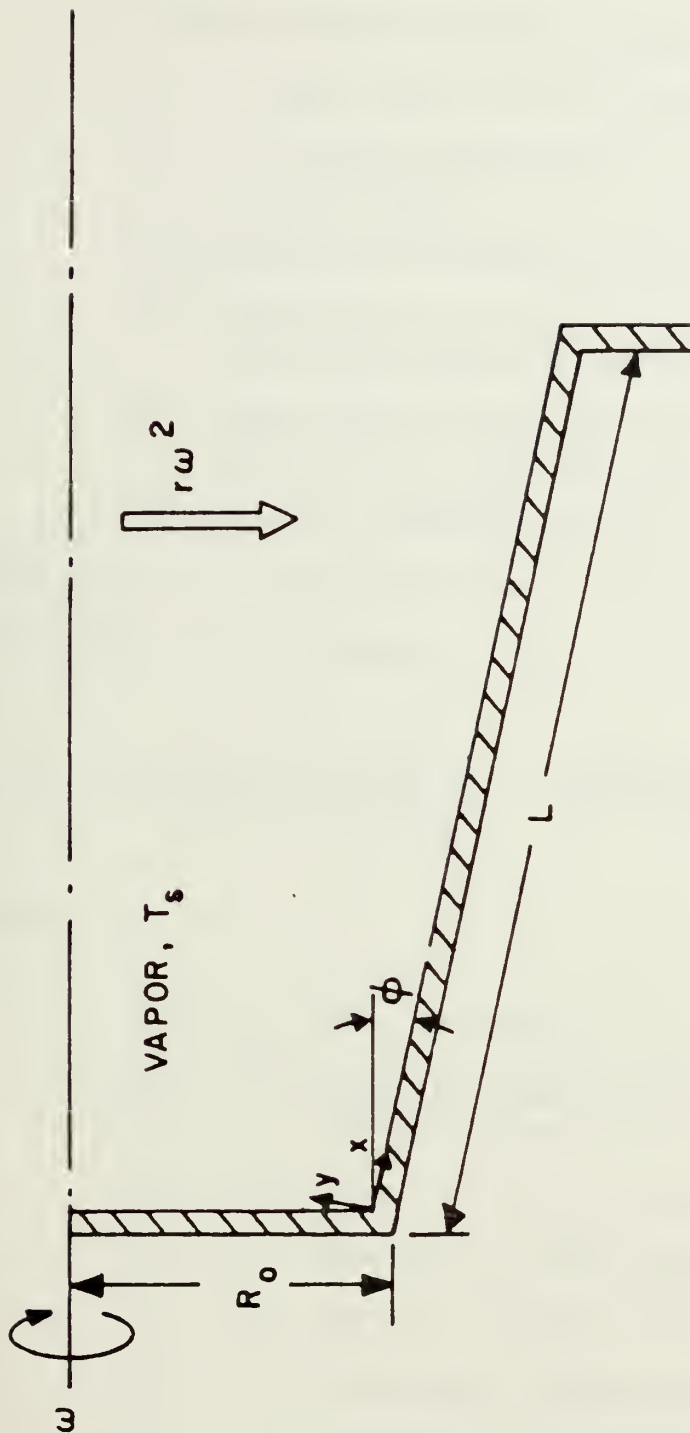


Figure 3. Coordinate System and Geometry for Laminar Film Condensation on a Rotating Truncated Cone

Additionally Ballback assumed:

- 11) a very small film thickness, $\delta(x)$,
- 12) no radial distribution of pressure in the vapor space,
- 13) negligible density of the vapor,
- 14) negligible velocity gradients in the circumferential direction, and
- 15) very small slope of the condensate film, $d\delta/dx$ when compared with $\tan \phi$.

He used the boundary condition, that $\delta(x)$ must be zero at $x = 0$, and arrived at the following solution for the local film thickness:

$$\delta(x) = \left\{ \frac{3}{2} \frac{k_f \mu_f (T_s - T_w)}{\rho_f \omega^2 \sin \phi h_{fg}} \left[1 - \left\{ \frac{R_o}{R_o + x \sin \phi} \right\}^{8/3} \right]^{1/4} \right\} \quad (12)$$

where

- $\delta(x)$ = film thickness, ft
- k_f = thermal conductivity of the fluid, BTU/hr-ft-deg F
- μ_f = viscosity of the fluid, lbm/ft-hr
- ρ_f = density of fluid, lbm/ft³
- ω = angular velocity, 1/hr
- T_w = inside wall temperature, deg F
- T_s = saturation temperature, deg F
- h_{fg} = latent heat of vaporization, BTU/lbm
- ϕ = half cone angle, degrees
- R_o = minimum wall radius in the condenser section, ft.

The local heat transfer coefficient, $h(x)$, is given by:

$$h(x) = \frac{k_f}{\delta(x)} = \left\{ \frac{2}{3} \frac{k_f^3 \rho_f^2 \omega^2 \sin \phi h_{fg}}{\mu_f (T_s - T_w)} \frac{1}{\left\{ 1 - \left[\frac{R_o}{R_o + x \sin \phi} \right]^{8/3} \right\}} \right\}^{1/4} \quad (13)$$

The mean heat transfer coefficient over the whole surface area of the truncated cone is given by:

$$h_m = \frac{1}{\pi L \{2R_o + L \sin \phi\}} \int_0^L 2\pi h(x) [R_o + x \sin \phi] dx \quad (14)$$

where

L = length along the wall of the condenser, ft.

Integrating equation (14) yields a value for the mean Nusselt number:

$$Nu_m = \frac{h_m L}{k} = 0.904 \left(\frac{\omega^2 L^2 R_o^2}{\nu^2} \frac{Pr}{C_p (T_s - T_w) / h_{fg}} \right)^{1/4} G(\beta) \quad (15)$$

where

$$G(\beta) = \frac{\{(1 + \beta)^{8/3} - 1\}^{3/4}}{\sqrt{\beta}(2 + \beta)}, \quad (16)$$

and

$$\beta = \frac{L \sin \phi}{R_0} .$$

Equation (15) can be put into the form:

$$Nu_m = (Nu_m)_{SH} \frac{G(\beta)}{\sqrt{\beta}} \quad (17)$$

where $(Nu_m)_{SH}$ is the result of Sparrow and Hartnett [5] for a cone, as given by equation (10). The above result was confirmed as a special case of the later work of Dhir and Lienhard [8], who studied laminar film condensation on axisymmetric bodies in nonuniform gravity fields.

Daley [9] was able to improve on the theory introduced by Ballback by consideration of the thermal resistances in the condenser wall and on the outside surface. Both Ballback and Daley, however, neglected the drag due to vapor friction on the counterflowing condensate film.

Newton [10] extended the analysis performed by Ballback and Daley to include the effects of vapor pressure drop and interfacial shear stress between vapor and condensate. Using the same geometry in Figure 3, he assumed that the momentum changes within the condensate film were small and arrived at the following differential equations for condensate film thickness, vapor velocity and heat transfer rate:

$$\frac{d\delta}{dx} = \tan \phi - \frac{\rho_v f v(x) \left[\frac{P_1(x)}{R(x)} + \frac{P_2(x)}{2} \right] + \rho_v v(x) \left[\frac{\mu_f^2 R(x)}{2\rho_f} - 2P_1(x) \frac{dv}{dx} \right]}{P_1(x) \cos \phi [\rho_f \omega^2 R(x) + \frac{2\rho_v v(x)}{R(x)}]} \quad (18)$$

$$\frac{dv}{dx} = \frac{2(R_o + x \sin \phi) (T_s - T_\infty)}{\rho_v \left[\frac{\delta(x)}{k_f} + \frac{t}{k_w} + \frac{1}{h} \right] h_{fg} R(x)} - \frac{2v(x)}{R(x)} [\sin \phi - \cos \phi \frac{d\delta}{dx}] \quad (19)$$

$$\frac{dq}{dx} = \frac{2\pi(R_o + x \sin \phi) (T_s - T_\infty)}{\frac{\delta(x)}{k_f} + \frac{t}{k_w} + \frac{1}{h}} \quad (20)$$

where

$$P_1(x) = (R_o + x \sin \phi) \frac{\delta^3(x)}{3} - \frac{5}{24} \cos \phi \delta^4(x),$$

$$P_2(x) = (R_o + x \sin \phi) \frac{\delta^2(x)}{2} - \cos \phi \frac{\delta^3(x)}{3},$$

$$v(x) = \text{velocity of vapor, ft/hr}$$

$$T_s = \text{saturation temperature of vapor, deg F}$$

$$T_\infty = \text{ambient coolant temperature, deg F}$$

$$t = \text{thickness of the condenser wall, ft}$$

$$\delta(x) = \text{film thickness of the condensate, ft}$$

$$k_f = \text{thermal conductivity of condensate film, BTU/hr-ft-deg F}$$

- k_w = thermal conductivity of condenser wall, BTU/hr-ft-deg F
 h = external heat transfer coefficient, BTU/hr-ft²-deg F
 h_{fg} = latent heat of vaporization, BTU/lbm
 f = friction factor, dimensionless,
 Re = vapor Reynolds number, $2R(x)\rho_v v(x)/\mu_v$
 $R(x)$ = radius along the condenser wall, $R_o + x\sin\phi - \delta\cos\phi$
 ϕ = half cone angle, degrees
 ρ_v = density of vapor, lbm/ft³
 μ_v = viscosity of vapor, lbm/ft-hr.

The integrations were started by assuming initial conditions $\delta = \delta_i$ and $v = 0$ at $x = 0$. With these initial conditions $\frac{d\delta}{dx} = \tan\phi$ at $x = 0$. Newton obtained results for half cone angles of 0, 0.1, 0.2 and 0.3 degrees. As the half cone angle increased, the solution of the differential equations became extremely sensitive to the initial values of δ_i . He also noted that his results for $\delta(x)$ showed that (except near the ends of the condenser) $\frac{d\delta}{dx} \ll \tan\phi$. He, therefore, made this approximation and simplified the model further using an order of magnitude analysis of the terms in equations (18) and (19). With these simplifications, equations (18) and (19) were reduced to:

$$\frac{dv}{dx} = \frac{2(R_o + x \sin \phi)(T_s - T_\infty)}{\rho_v \left(\frac{\delta(x)}{k_f} + \frac{t}{k_w} + \frac{1}{h} \right) h_{fg} R(x)^2} - \frac{2v(x) \sin \phi}{R(x)} \quad (21)$$

$$\begin{aligned} \frac{\delta(x)^3}{3} R(x) \sin \phi [\rho_f \omega^2 R(x) + \frac{2\rho_v v(x)}{R(x)}] - \rho_v v(x)^2 f [R(x) \frac{\delta(x)^2}{4}] \\ - \rho_v v(x) \frac{\mu_f R(x)}{2\rho_f} = 0 \end{aligned} \quad (22)$$

Equation (21) was numerically integrated using the initial condition that $\delta_i = 0$ and $v = 0$ at $x = 0$ and using the cubic equation for $\delta(x)$, equation (22). After the integration was completed for $\delta(x)$ and $v(x)$, the energy equation, equation (20), was integrated over the length of the condenser to find the total heat transfer rate of the heat pipe. This theory was compared to the experimental results of Schafer [15] and Tucker [20], predicting performance to within ± 20 percent for water, ethyl alcohol and Freon 113.

Daniels and Al-Jumaily [11,12] extended the analysis of Ballback by including drag effects due to the vapor friction. Their solution for the local film thickness distribution along the condenser is given by:

$$Sh_x \left[\frac{\delta(x)}{x} \right]^4 - \frac{1}{3} Dr_x \left[\frac{\delta(x)}{x} \right]^3 - \frac{1}{4} Re_{vx} \left[\frac{\delta(x)}{x} \right]^2 - 1 = 0 \quad (23)$$

where

$$Sh_x = \text{Sherwood number, } \frac{\rho^2 (\omega r - g) \sin \phi h_{fg} x^3}{4 \mu k \Delta T}$$

$$Dr_x = \text{drag friction number, } \frac{\rho \tau_v h_{fg} x^2 \cos \phi}{\mu k \Delta T}$$

$$Re_{vx} = \text{two phase Reynolds number, } \frac{\rho u_v x \cos \phi}{\mu}$$

$$\rho = \text{liquid density, lbm/ft}^3$$

$$\delta(x) = \text{film thickness, ft}$$

$$\omega = \text{angular velocity, 1/hr}$$

$$\phi = \text{half cone angle, degrees}$$

$$\tau_v = \text{shear stress at liquid vapor interface, lbf/ft}^2$$

$$u = \text{liquid condensate velocity, ft/hr}$$

$$g = \text{acceleration of gravity, ft/hr}^2$$

$$h_{fg} = \text{latent heat of vaporization, BTU/lbm.}$$

At any section x in the condenser, since heat is transferred through the condensate layer by conduction only, the local heat flux $Q_x = k \Delta T / \delta(x)$ and equation (23) can be re-arranged as follows:

$$Q_x^4 + \frac{1}{4} Re_{vx} \left(\frac{k \Delta T}{x} \right)^2 Q_x^2 + \frac{1}{3} Dr_x \left(\frac{k \Delta T}{x} \right)^3 Q_x - Sh_x \left(\frac{k \Delta T}{x} \right)^4 = 0 \quad (24)$$

where

$$Q_x = \text{local heat flux, BTU/hr-ft}^2.$$

This equation relates the three main parameters controlling the rotating heat pipe operation assuming fixed geometry and working fluid. The mean Nusselt number, Nu_m , for this analysis was,

$$Nu_m = \frac{4}{3} Sh_L \left(\frac{\delta_L}{L}\right) - \frac{1}{2} Dr_L \left(\frac{\delta_L}{L}\right)^2 - \frac{1}{2} Re_{vL} \left(\frac{\delta_L}{L}\right) \quad (25)$$

where suffix L refers to quantities evaluated at the end of the condenser section $x = L$.

Marto [13] compared the heat transfer rates of Daniels and Al-Jumaily with Ballback and the approximate numerical solution to equations (20), (21) and (22). For the case of Freon 113, equations (20), (21) and (22), which include both effects of interfacial shear as well as vapor pressure drop, gave slightly lower heat transfer rates than the analysis of Daniels and Al-Jumaily which includes only interfacial effects. Also the analysis of Ballback predicts slightly larger results than the computer analysis but lower results than those of Daniels and Al-Jumaily. This may be due to differences in the Freon 113 fluid properties used or due to the geometrical inconsistency in matching all the geometrical dimensions as stated in the analysis of Daniels and Al-Jumaily. For the case of water,

Ballback's results again predict a slightly higher heat transfer rate than the approximate numerical solution, due to his neglecting effects of interfacial shear and vapor pressure drop. When these effects are neglected in the approximate numerical solution, the results agree very well with those of Ballback. For these reasons, the effects of interfacial shear and vapor pressure drop can safely be neglected.

Roetzel [14] studied condensation in steam heated fast rotating paper drying drums, as shown in Figure 4. In his analysis, the heat transfer is determined mainly by the method of condensate removal. The condensate is collected in a circumferential groove on the inside surface, and from there it is removed by means of a stationary syphon with its tip in the groove. The mean film thickness is slightly smaller than with a rotating syphon because the condensate is sucked off from a lower level. The solution for the case of a drum with an infinite radius of curvature (The inside surface is exactly cylindrical.) with a uniform temperature difference is given by:

$$\text{Nu}_{\infty} = (0.86 E)^{1/5} \quad (26)$$

where

Nu_{∞} = Nusselt number for the cylindrical drum,

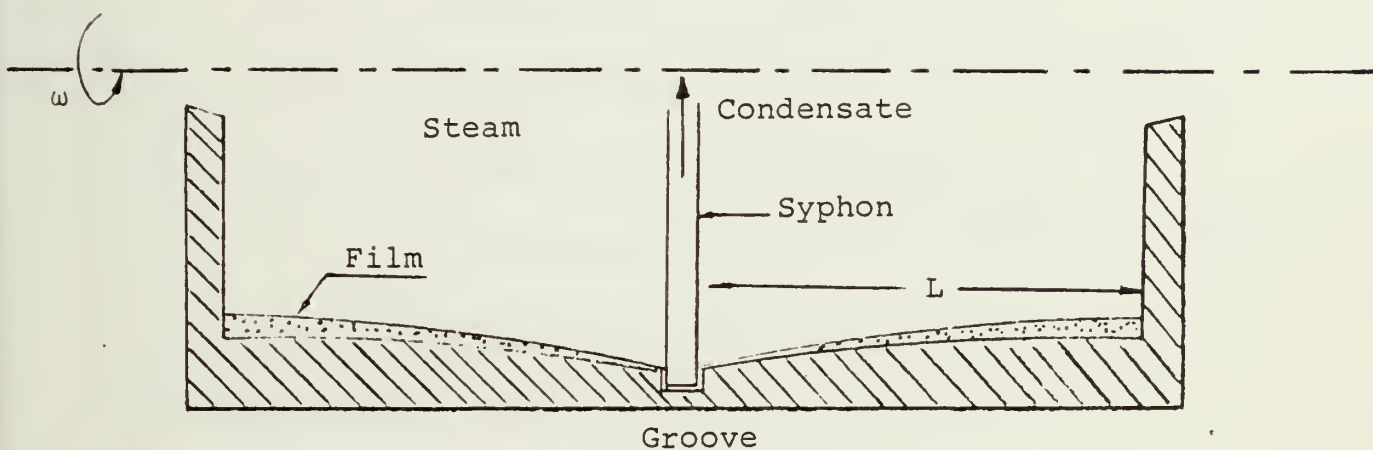


Figure 4. Schematic Drawing of Paper Drying Drum with Two Curved Conical Sections and One Sampling Groove

$$E = 1/6 \text{ Sh} = \frac{b_n \rho h_{fg} L^3}{6 \nu k_f \Delta T_m}$$

k_f = thermal conductivity of condensate, BTU/hr-ft-deg F

Sh = Sherwood number

b_n = acceleration normal to the wall, ft/hr²

ρ = density of condensate, lbm/ft³

h_{fg} = latent heat of vaporization, BTU/lbm

L = total length of condensate, ft

ν = kinematic viscosity of condensate, ft²/hr.

This equation can be written in terms of the Sherwood number:

$$\text{Nu}_\infty = 0.678 \text{ Sh}^{1/5} \quad (27)$$

and compares favorably to the analysis of Nimmo and Leppert, equation (11).

For the case of finite radius of curvature, Roetzel's solution becomes:

$$\text{Nu}_m = \left[\left(\frac{2LE}{R} \right)^{23/16} + (0.86E)^{23/20} \right]^{4/23} \quad (28)$$

where

R = radius of curvature, ft, and

L = total flow length of condenser, ft.

This equation can be put in terms of Sh , Nu_{∞} , R , and L as:

$$Nu_m = Nu_{\infty} [1 + 1.924 \left(\frac{L}{R}\right)^{23/16} Sh^{23/80}]^{4/23} . \quad (29)$$

Thus the Nusselt number can be directly determined when the ratio L/R and the value of the dimensionless group, E , are known. For the truncated cone, rotating heat pipe, as shown in Figure 3, equation (29) can be applied to compute the heat transfer by defining the radius of curvature $R = L/\tan \phi$; the solution then becomes:

$$Nu_m = Nu_{\infty} [1 + 1.924 \tan \phi^{23/16} Sh^{23/80}]^{4/23} \quad (30)$$

where

ϕ = half cone angle, degrees

Nu_{∞} = Nusselt number of the cylindrical drum,
equation (11).

Equation (30) has never been compared with experimental data, so using the existing rotating heat pipe data together with new experimental data at different half cone angles will provide a check on its usefulness.

These theoretical investigations are summarized below:

1. The vapor pressure drop and interfacial shear stress effects between vapor and condensate can be neglected.
2. The analysis of Roetzel [14] appears to be the most appropriate for use in a rotating heat pipe.
3. The important parameters are:
 - (a) speed,
 - (b) geometry, and
 - (c) Sherwood number, which includes the properties of the working fluid.

D. ANALYSIS OF FINNED ROTATING CONDENSER SURFACES

The use of axial fins on the inner surface of the condenser can improve heat transfer performance through two mechanisms: a decrease in condensate film thickness near the apex of each fin and an increase in inner wall surface area. Schafer [15] developed an analytical model of the internally finned condenser for the case of a fin of triangular profile as shown in Figure 5, with a specific geometry as shown in Figure 6. In the analysis, he assumed one-dimensional heat conduction from the inside to the outside surface and a linearly decreasing surface temperature profile from the fin apex to the midpoint of the trough. Results from his analysis indicated significantly

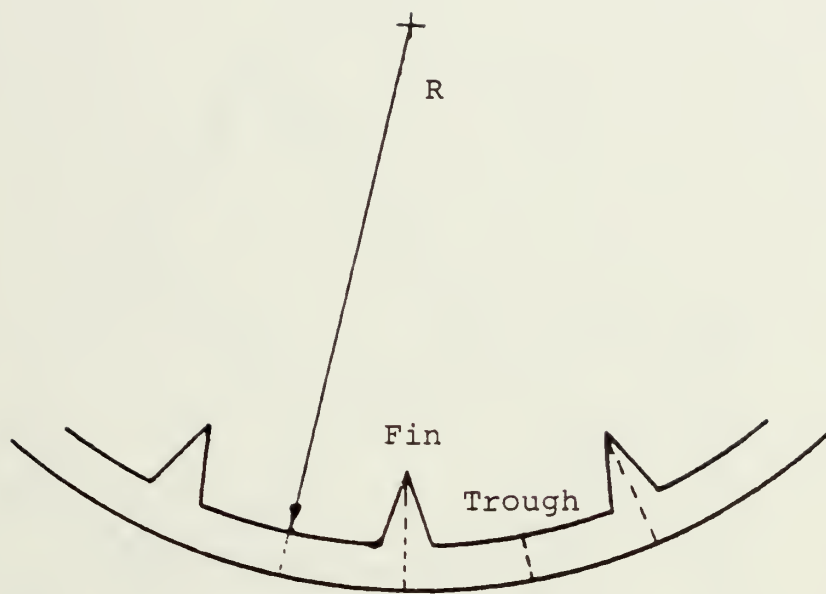


Figure 5. Internally Finned Condenser Geometry
Showing Fins, Troughs and Lines of Symmetry

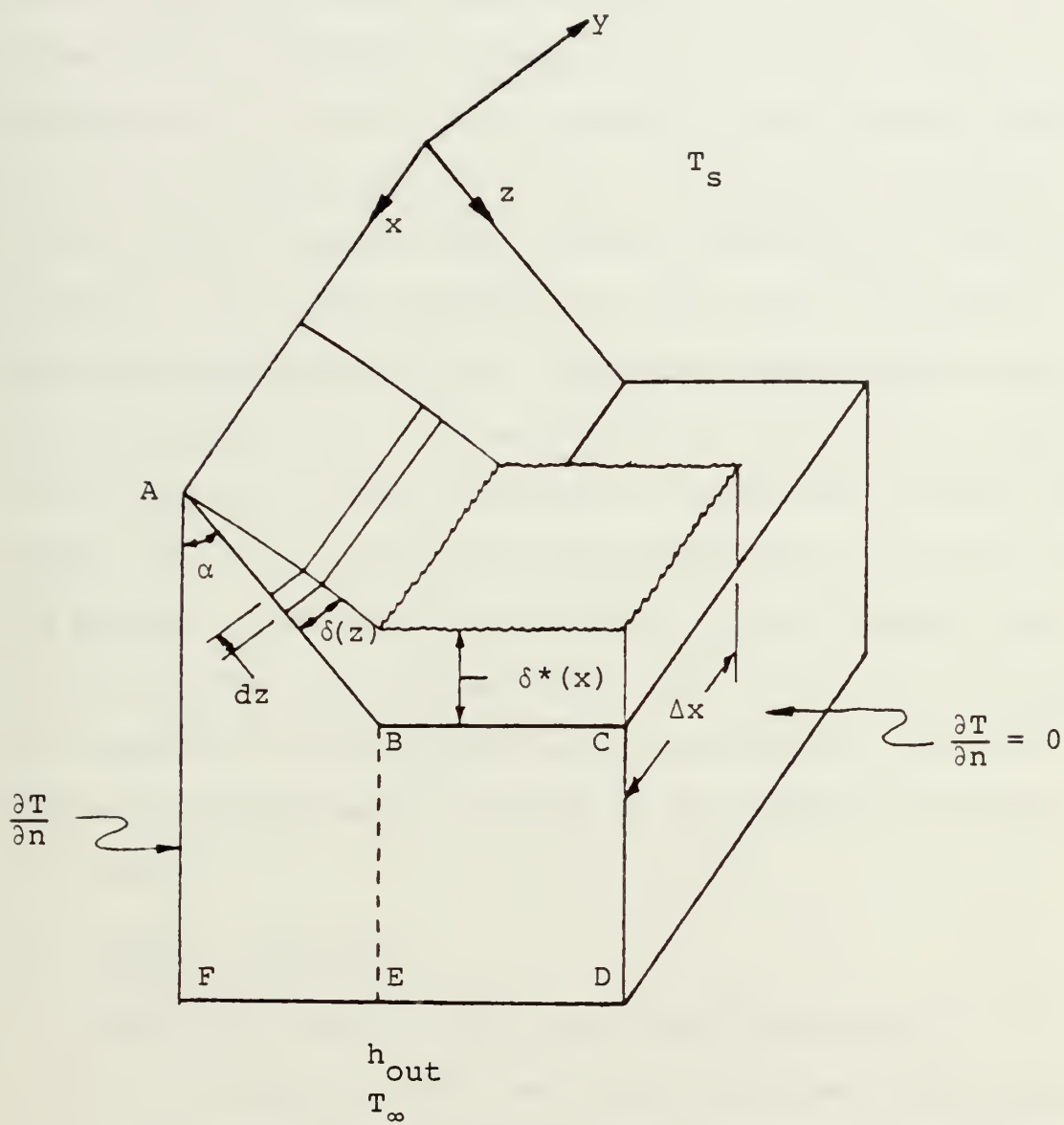


Figure 6. Condenser Geometry Considered in Analysis

improved heat transfer rates for the finned condenser compared to the smooth condenser.

Corley [16] developed a numerical solution for this case using the Finite Element method to account for two-dimensional conduction effects within the wall for the triangular fin profile and a parabolic wall surface temperature distribution along the fins. His results indicated significantly improved heat transfer performance with heat transfer rates about 75 percent above those predicted by the one-dimensional linear temperature distribution analysis of Schafer [15]. However, Corley noted that an error of 50 percent in the calculation of apex heat transfer rate might then give a total heat transfer error of as high as 15 percent. Two possible solutions to the boundary condition problem were recommended. The first was to increase the number of Finite Elements in the analysis, and the second solution was to consider a wall geometry as shown in Figure 7.

E. THESIS OBJECTIVES

The objectives of this thesis were therefore:

- 1) to find out which existing theory best correlates Rotating Heat Pipe data by comparing these theories with existing data and new experimental data of this thesis, and
- 2) to further study finned condensers by improving the Finite Element results obtained earlier.

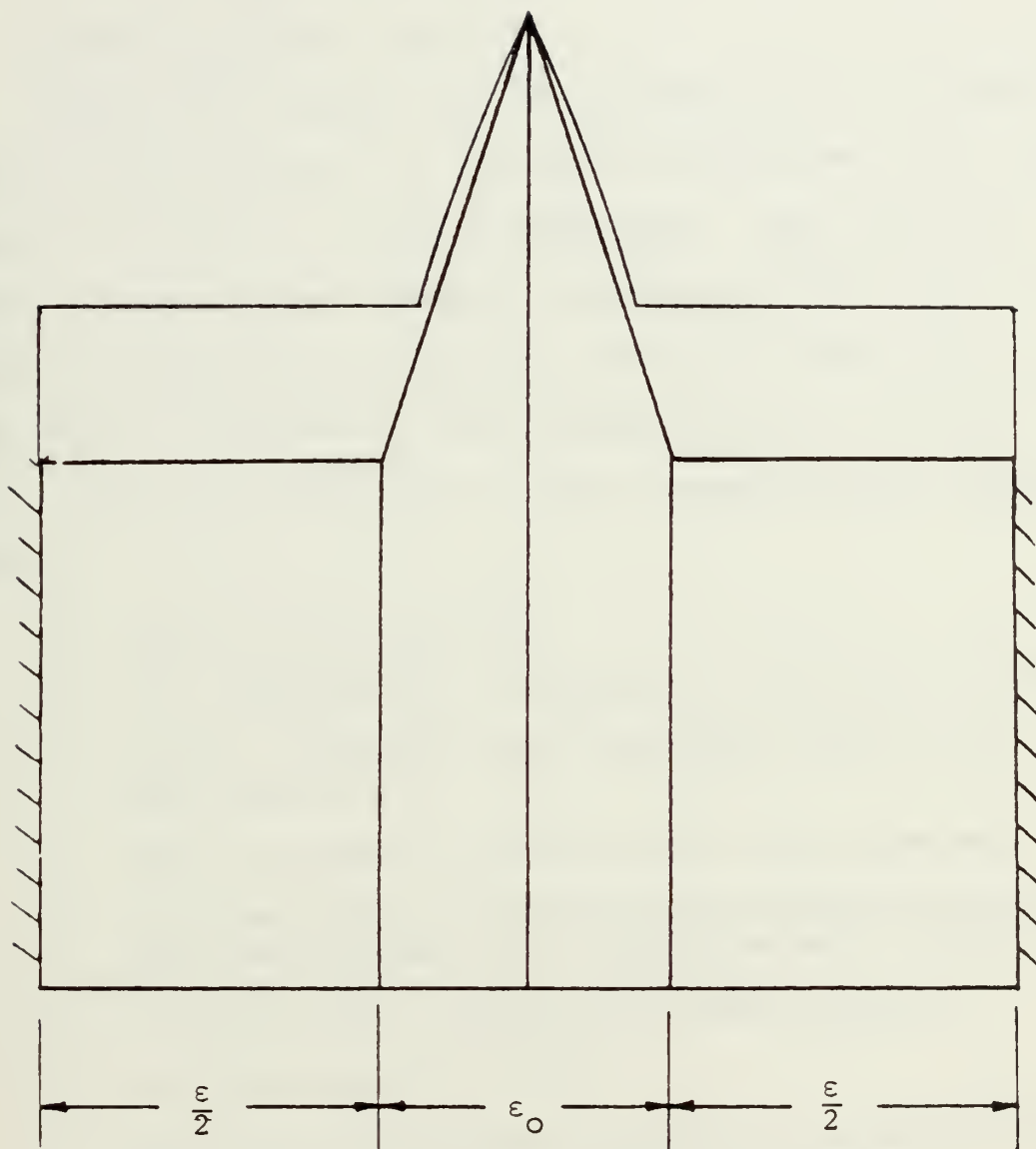


Figure 7. Alternate Condenser Wall Geometry

II. FINITE ELEMENT ANALYSIS AND RESULTS

A. REVIEW OF EARLIER ANALYSES

Schafer [15] studied the one-dimensional heat transfer solution, and Corley [16] studied the two-dimensional heat transfer solution to finned condensers. Both used the same assumptions and boundary conditions, based upon the work of Ballback [1], which are similar to those used in the Nusselt analysis of film condensation on a vertical wall. The more important of these assumptions are listed below:

- 1) steady state operation,
- 2) film condensation, as opposed to dropwise condensation,
- 3) laminar condensate flow along both the fin and the trough,
- 4) static balance of forces within the condensate,
- 5) one-dimensional conduction heat transfer through the film thickness (no convective heat transfer),
- 6) no liquid-vapor interfacial shear stresses,
- 7) no condensate subcooling,
- 8) zero heat flux boundary conditions on both sides of the wall section, as shown in Figure 6,
- 9) saturation temperature at the fin apex,
- 10) zero film thickness at the fin apex,
- 11) negligible curvature of the wall.

The complete development of Schafer's finned condenser heat transfer theory is presented in his thesis [15]. His

results are used for comparison purposes in this thesis.

Corley's study [16] considered an internal fin geometry as shown in Figure 6. Two-dimensional conduction through the condenser wall was considered in the heat transfer analysis by using a Finite Element solution. Instead of using a linearly decreasing temperature profile along the wall from the apex of the fin to the midpoint of the channel as Schafer did, a parabolic distribution was assumed to calculate average nodal convective coefficients. The eight node finite element mesh used in the two-dimensional analysis of the axially finned condenser is shown in Figure 8. A computer program for the case of two-dimensional conduction was developed using a modified version of the three dimensional, isoparametric Finite Element program assembled by Lew [17].

A parabolic temperature distribution is assumed to exist along the fin surface using the boundary condition, $T = T_s$ at $z = 0$, since $\delta(0) = 0$. Therefore;

$$T_w(z) = a_1 z^2 + b_1 z + T_s$$

or

$$T_s - T_w(z) = -a_1 z^2 - b_1 z \quad (31)$$

where

a_1 and b_1 are unknown constants, and

z is the distance along fin surface from apex of fin, ft.

From Schafer's analysis [15] a differential equation for fin condensate thickness, $\delta(z)$, can be derived:

$$\delta^3(z) d\delta(z) = \frac{k_f (T_s - T_w(z)) \mu_f dz}{\rho_f^2 \omega^2 (R_o + x \sin \phi) h_{fg} \cos \phi \cos \alpha} \quad (32)$$

where

$\delta(z)$ = the fin condensate thickness, ft

k_f = thermal conductivity of working fluid, BTU/hr-ft-deg F

ρ_f = density of working fluid, lbm/ft³

μ_f = viscosity of working fluid, lbm/ft-hr

ω = angular velocity, 1/hr

R_o = minimum radius, ft

x = distance along apex of fin, ft

z = distance along the fin, from the apex, ft.

ϕ = half cone angle, degrees

α = fin half-angle, degrees

h_{fg} = latent heat of vaporization, BTU/lbm.

Equation (31) is then substituted in (32), and the result is integrated from $z = 0$ to z to give an equation for $\delta(z)$:

$$\delta(z) = \left[\frac{4k_f(-a_1 \frac{z^3}{3} - b_1 \frac{z^2}{2}) \mu_f}{\rho_f^2 \omega^2 (R_o + x \sin \phi) h_{fg} \cos \phi \cos \alpha} \right]^{1/4}, \quad (33)$$

The local convective heat transfer coefficient assuming one-dimensional heat conduction through the thin condensate film is then:

$$h(z)_{fin} = \frac{k_f}{\delta(z)} = \left[\frac{k_f^3 \rho_f^2 \omega^2 (R_o + x \sin \phi) h_{fg} \cos \phi \cos \alpha}{4 \mu_f (-a_1 \frac{z^3}{3} - b_1 \frac{z^2}{2})} \right]^{1/4} \quad (34)$$

which is applicable from $z = 0$ to $z^* = z_o - \delta^*/\cos \alpha$, where δ^* is the trough condensate thickness, as shown in Figure 8. Across the width of trough, from $z = z_o$ to the mid channel position, the heat transfer coefficient is:

$$h(x)_{trough} = \frac{k_f}{\delta^*(x)} \quad (35)$$

where $\delta^*(x)$ is considered constant across the trough width. Based upon a check of the wall temperatures generated from Schafer's computer program, the fluid temperature difference across the width of the trough was predicted to be small.

Fluid thermal conductivity values were assumed to remain relatively constant. As a result, $h(x)_{\text{trough}}$ is assumed to be constant across the trough width and is calculated using equation (35) and a representative average inner wall temperature to determine k_f . The convective coefficient along the outside surface of the wall, h_{out} , is also assumed to be constant. The modified trough mass flow equation becomes:

$$\dot{M}_{\text{tot}}(x) = \frac{\rho^2 \omega^2 (R_o + x \sin \phi)^2 \delta^*(x) \sin \phi}{3 \mu_f} [\delta^*(x) \epsilon + \delta^*(x) \tan \alpha] \quad (36)$$

Within the computer program, the heat transfer rate for the entire condenser is determined by dividing its axial length into one hundred equal length increments of length, Δx (See Figure 6.), solving for the incremental heat transfer rate using an iterative procedure, and summing these incremental rates to yield a total heat transfer rate. A flow chart description of the computer program used in Corley's analysis is given in Figure 9. At each increment, constant values of a_1 and b_1 are determined using a Lagrangian interpolation fit of the temperatures, at nodes 1, 3 and 6 as calculated from the previous iteration. For the first increment, a_1 and b_1 are calculated from an initial guess of the temperatures at these nodes. Convective coefficients at several locations along

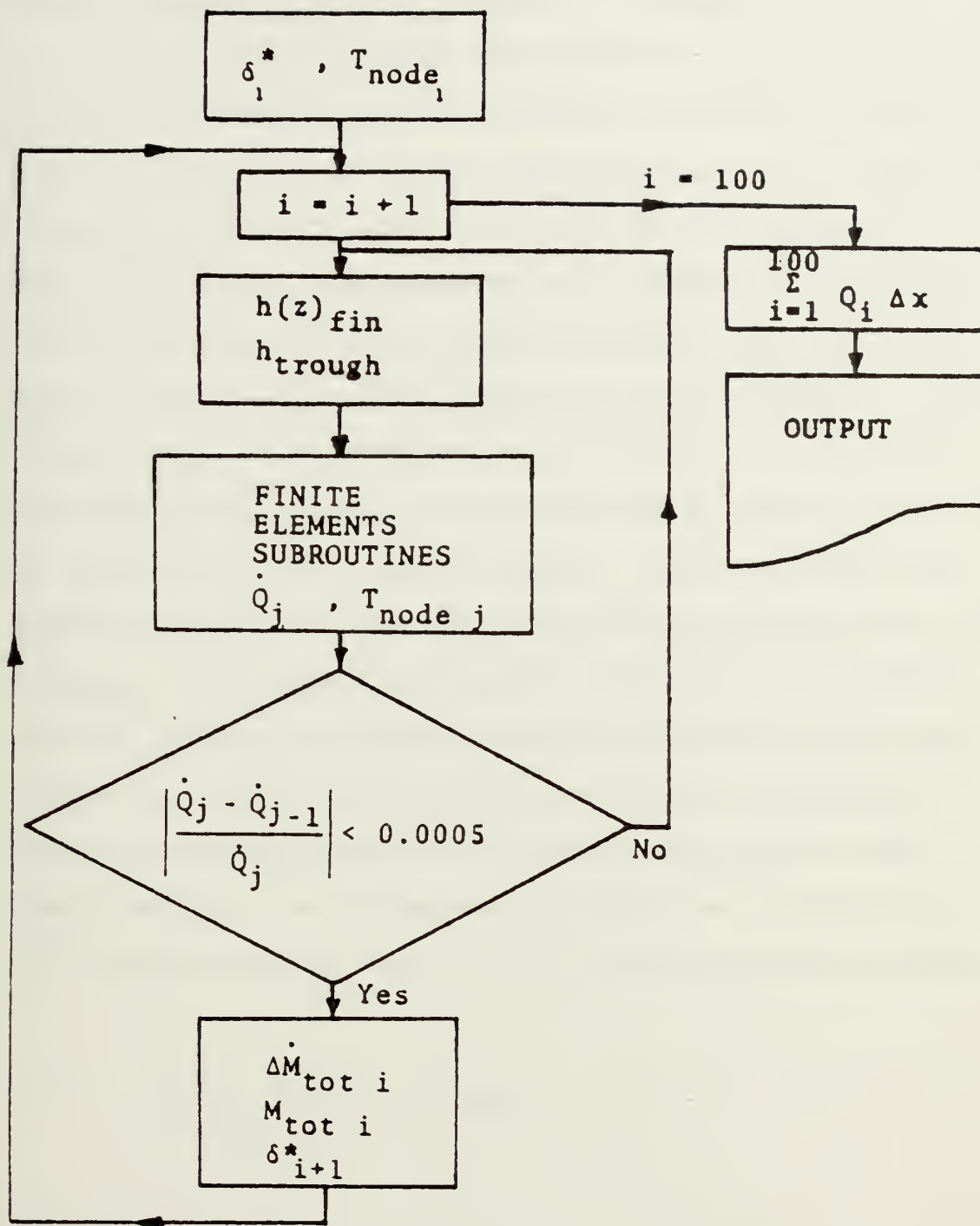


Figure 9. Computer Program Flowchart of Two-Dimensional Conduction Analysis of Corley [16]

the fin are determined using equation (34). Average nodal values, h_{1avg} , h_{3avg} , and the average h of the left-hand boundary region associated with node 6, in Figure 8, are calculated using the position dependent values of $h(z)_{fin}$ in a Simpson's Rule approximation. In the trough, $h(x)_{trough}$ is calculated from equation (35) using the δ^* value calculated from the previous increment. This value is used as the average convective coefficient for nodes 9 and 12 and the right hand boundary region of node 6. The average convective coefficients calculated for the left- and right-hand boundary regions of node 6 are weighted by their respective region lengths. The two values are summed to yield the average convective coefficient for node 6, h_{6avg} . The remaining boundary conditions are applied, and the incremental heat transfer rate per unit condenser length, \dot{Q}_j , and nodal temperature values are generated from the finite element subroutines. If the resultant heat transfer rate converges to within the criterion of 0.05 percent change from the value of the previous iteration,

$$\left| \frac{\dot{Q}_j - \dot{Q}_{j-1}}{\dot{Q}_j} \right| \ll 0.0005 , \quad (37)$$

then the incremental problem is deemed solved and \dot{Q}_1 is set equal to the final iteration, \dot{Q}_j . If, on the other hand, the convergence criteria is not met, newly calculated

nodal temperature values are used to establish a new set of inner wall convective coefficients, and the finite element solution is repeated until the heat transfer rate converges to within the acceptable 0.05 percent tolerance. Because \dot{Q}_j is initialized at zero for each increment, the iteration procedure is repeated at least twice for every increment. Incremental mass flow rate is calculated using:

$$\Delta \dot{M}_{\text{tot}} = 2 \frac{\dot{Q}_i}{h_{fg}} \Delta x \quad (38)$$

This value is added to the mass flow rate from previous increments. The subsequent interval's trough condensate thickness, $\delta^*(x)$, is calculated using a polynomial root-finder subroutine to solve equation (36). This incrementation is continued until the entire length of the condenser is traversed. Incremental heat transfer rates are summed, and a total heat transfer rate becomes:

$$\dot{Q}_{\text{tot}} = 2 N_{\text{fin}} \sum_{i=1}^{100} (\dot{Q}_i \Delta x) \quad (39)$$

where N_{fin} is the number of fins along the inner wall circumference. To start the incrementation, two initial assumptions are made. The initial value of $\delta^* = \delta_i^*$ is taken from the analysis by Sparrow and Gregg of condensation on a rotating disk [4]. In addition, at the first increment, initial guesses of fin temperatures at nodes 1, 3 and 6 are made in order to begin the solution.

B. MODIFICATION TO THE FINITE ELEMENT ANALYSIS

This thesis is a continuation of Corley's [16] study of the addition of internal axial fins to the condenser surface of a rotating heat pipe. He recommended that one way to approximate more closely the actual heat transfer rates would be by increasing the number of elements for the same geometry. Since Corley used one hundred equal increments of length to compute the heat transfer rates, the first step in this thesis was to reduce the number of increments to fifty and twenty five, to minimize the computer time. Using Corley's program, at a speed of 3000 RPM, with external convective coefficients of 1000, 1500 and 5000 BTU/hr-ft²-deg F and fin half angles of 10, 30 and 50 degrees, the results for water as the working fluid are shown in Tables 2, 3 and 4. It is clear that reducing the number of increments to twenty five had little effect upon the heat transfer results (approximately 3 percent error).

To reduce any error in the calculation of the heat transfer rate at the apex of the fin, the number of Finite Elements has to be increased between the apex of the fin and the trough, as shown in Figure 10. The geometry becomes 3 elements and 18 nodes. The computer program was therefore modified to solve this case, using the same boundary conditions and assumptions. These results are shown in Tables 5 through 10. Upon dividing element ① in Figure 10 into

TABLE 2

Theoretical Finned Condenser Heat Transfer
Rate Versus Number of Axial Increments

$$h_{\text{out}} = 1000 \text{ BTU/hr-ft}^2\text{-deg F}$$

At 3000 RPM

Fin Half Angle	No. of Fins	T_{sat}	No. of Axial Increments		
			25	50	100
10	276	100	10273.1	10039.0	9922.5
		150	27355.8	26732.6	26422.4
		200	44427.2	43415.0	42911.2
30	84	100	10095.3	9865.3	9750.8
		150	26866.0	26253.8	25949.1
		200	43622.0	42627.9	42133.2
50	40	100	9870.9	9643.5	9530.3
		150	26255.7	25650.8	25349.9
		200	42623.3	41641.2	41152.6

TABLE 3

Theoretical Finned Condenser Heat Transfer
Rate Versus Number of Axial Increments

$$h_{\text{out}} = 1500 \text{ BTU/hr-ft}^2\text{-deg F}$$

At 3000 RPM

Fin Half Angle	No. of Fins	T_{sat}	No. of Axial Increments		
			25	50	100
10	276	100	15195.2	14849.2	14677.1
		150	40427.4	39507.2	39049.2
		200	65632.8	64138.9	63395.3
30	84	100	14808.4	14471.6	14304.0
		150	39368.6	38473.3	38027.8
		200	63896.8	62443.8	61720.6
50	40	100	14368.5	14038.7	13874.6
		150	38174.4	37298.1	36862.1
		200	61943.9	60521.6	59814.1

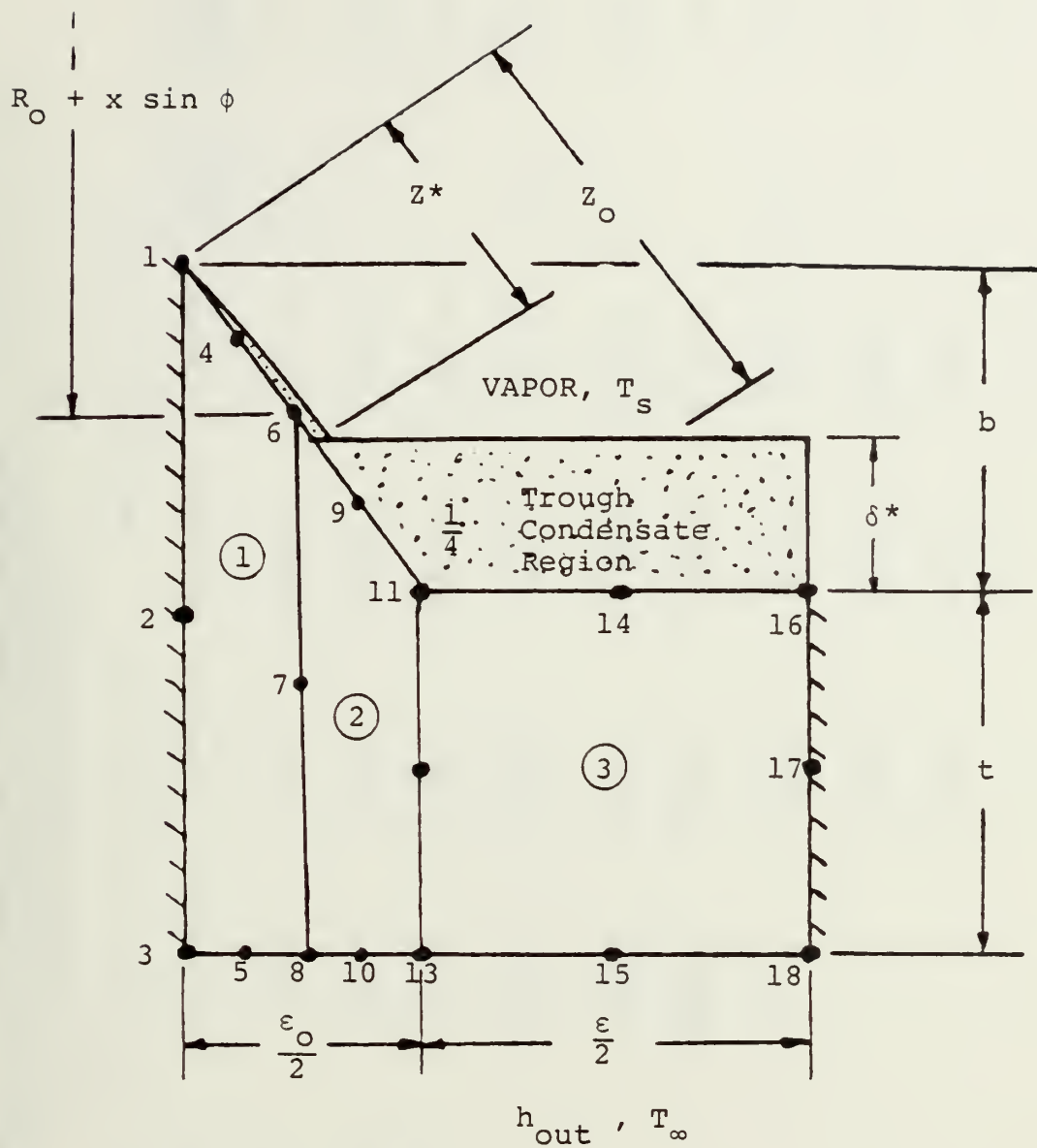
TABLE 4

Theoretical Finned Condenser Heat Transfer
Rate Versus Number of Axial Increments

$$h_{\text{out}} = 5000 \text{ BTU/hr-ft}^2\text{-deg F}$$

At 3000 RPM

Fin Half Angle	No. of Fins	T_{sat}	No. of Axial Increments		
			25	50	100
10	276	100	45685.4	44652.3	44138.1
		150	120807.7	118075.1	116715.1
		200	195703.4	191270.2	189066.4
30	84	100	42327.3	41377.0	40904.1
		150	111871.5	109356.8	108106.0
		200	181198.5	177121.2	175092.6
50	40	100	39287.1	38402.4	37962.4
		150	103724.0	101386.0	100222.1
		200	167950.6	164155.9	162268.8



$$\begin{aligned}
 t &= 0.03125 \text{ in.} \\
 b &= 0.025 \text{ in.} \\
 R_o &= 0.762 \text{ in.} \\
 \phi &= 1^\circ
 \end{aligned}$$

Figure 10. Condenser Geometry Considered in Two-Dimensional Analysis with 3 Finite Elements

TABLE 5

Comparison of Theoretical Finned Condenser
Heat Transfer Rate at 1000 RPM, for
 $h_{out} = 1000 \text{ BTU/hr-ft}^2\text{-deg F}$

Fin Half Angle	No. of Fins	T_{sat}	Schafer [15] Corley [16]				Results of This Thesis	
			Schafer smooth	1-dimension	2 Elements	3 Elements	4 Elements	$\frac{A_4 \text{ Element}}{A \text{ Smooth}}$ $\frac{Q_4 \text{ Element}}{Q \text{ Smooth}}$
10	276	100	4971.0	5720.0	10191.7	10161.4	10156.3	3.144 2.04
		150	12278.0	14914.0	27125.9	27027.7	27006.8	2.199
		200	19531.7	24072.0	44046.9	43878.6	43840.9	2.245
30	84	100		5697.0	9998.8	9952.7	9907.9	1.448 1.993
				14815.0	26611.7	26466.3	26320.3	2.144
				23888.0	43210.5	42960.1	42708.8	2.188
50	40	100			9758.7	9696.9	9626.0	1.128 1.936
		150			25965.8	25775.0	25555.0	2.081
		200			42156.4	41831.4	41459.3	2.123

TABLE 6

Comparison of Theoretical Finned Condenser
Heat Transfer Rate at 3000 RPM, for
 $h_{out} = 1000 \text{ BTU/hr-ft}^2\text{-deg F}$

Fin Half Angle	No. of Fins	T_{sat}	Schafer[15] smooth	Schafer[15] 1-Dimension	Corley[16] 2 Elements	3 Elements	4 Elements	Results of This Thesis	
								$\frac{A_4 \text{ Element}}{A \text{ Smooth}}$	$\frac{Q_4 \text{ Element}}{Q \text{ Smooth}}$
10	276	100	6474.7	6193.0	10273.1	10255.2	10256.9	3.144	1.584
		150	16420.0	16266.0	27355.8	27308.9	27310.8		1.663
		200	26287.7	26223.0	44427.2	44351.6	44353.4		1.687
30	84	100		6303.0	10095.3	10071.2	10059.6	1.448	1.554
		150		16224.0	26866.0	26795.9	26755.0		1.629
		200		26290.0	43622.0	43504.0	43431.4		1.652
50	40	100			9870.9	9836.9	9809.6	1.128	1.515
		150			26255.7	26155.0	26065.7		1.587
		200			42623.3	42452.9	42298.0		1.609

TABLE 7

Comparison of Theoretical Finned Condenser
Heat Transfer Rate at 1000 RPM, for
 $h_{out} = 1500 \text{ BTU/hr-ft}^2\text{-deg F}$

Fin Half Angle	No. of Fins	T_{sat}	Schafer[15] smooth	Schafer[15] 1-Dimension	Corley[16] 2 Elements	3 Elements	4 Elements	Results of This Thesis	
								$\frac{A_4 \text{ Element}}{A \text{ Smooth}}$	$\frac{Q_4 \text{ Element}}{Q \text{ Smooth}}$
10	276	100	5780.7	7978.0	15009.5	14931.6	14917.6	3.144	2.581
		150	13998.2	20764.0	39909.9	39683.0	39624.0		2.831
		200	22158.7	33488.0	64780.6	64398.8	64296.0		2.902
30	84	100		7866.0	14604.8	14493.7	14380.7	1.448	2.487
		150		20342.0	38839.7	38497.5	38141.7		2.725
		200		32729.0	63044.4	62459.6	61853.4		2.791
50	40	100			14139.5	13995.2	13828.0	1.128	2.392
		150			37588.9	37157.9	36656.0		2.619
		200			61004.6	60271.9	59424.5		2.682

TABLE 8

Comparison of Theoretical Finned Condenser
Heat Transfer Rate at 3000 RPM, for
 $h_{out} = 1500 \text{ BTU/hr-ft}^2\text{-deg F}$

Fin Half Angle	No. of Fins	T_{sat}	Schafer[15]			Corley[16]		Results of This Thesis			
			smooth	1-Dimension	2 Elements	3 Elements	4 Elements	$\frac{A_4 \text{ Element}}{A \text{ Smooth}}$	$\frac{Q_4 \text{ Element}}{Q \text{ Smooth}}$		
10	276	100	8030.3	8694.0	15195.2	15156.8	15158.7	3.144	1.889		
		150	19993.1	22698.0	40429.4	40328.4	40328.7		2.017		
		200	31856.2	36648.0	65632.8	65473.5	65471.6		2.055		
30	84	100		8675.0	14808.4	14752.8	14720.5	1.448	1.833		
		150		22608.0	39368.6	39205.2	39205.2		1.955		
		200		36482.0	63896.8	63620.7	63620.7		1.991		
50	40	100			14368.5	14290.0	14220.6	1.128	1.771		
		150			38174.4	37941.2	37717.6		1.887		
		200			61943.9	61549.7	61164.2		1.920		

TABLE 9

Comparison of Theoretical Finned Condenser
Heat Transfer Rate at 1000 RPM, for
 $h_{out} = 5000 \text{ BTU/hr-ft}^2\text{-deg F}$

Fin Half Angle	No. of Fins	T_{sat}	Schafer[15] smooth	Schafer[15] 1-Dimension	Corley[16] 2 Elements	3 Elements	4 Elements	Results of This Thesis	
								$\frac{A_4 \text{ Element}}{A}$	$\frac{Q_4 \text{ Element}}{Q \text{ Smooth}}$
10	276	100	7339.2	20983.0	43925.1	43160.3	42892.9	3.144	5.844
		150	17047.8	53680.0	116132.5	113809.4	112962.4		6.626
		200	26669.7	85619.0	188087.0	184090.4	182658.8		6.850
30	84	100		18794.0	40850.6	39745.0	38564.0	1.448	5.255
		150		46893.0	108189.1	104861.7	101354.7		5.945
		200		74539.0	175334.0	169675.6	163810.7		6.142
50	40	100			37808.3	36586.2	35173.2	1.128	4.793
		150			100094.8	96506.5	92429.3		5.422
		200			162188.9	156162.4	149403.1		5.602

Comparison of Theoretical Finned Condenser
Heat Transfer Rate at 3000 RPM, for
 $h_{out} = 5000 \text{ BTU/hr-ft}^2\text{-deg F}$

Fin Half Angle	No. of Fins	T_{sat}	Schafer[15] smooth	Schafer[15] 1-Dimension	Corley[16] 2 Elements	3 Elements	4 Elements	Results of This Thesis $\frac{A_4 \text{ Element}}{A \text{ Smooth}}$	$\frac{Q_4 \text{ Element}}{Q \text{ Smooth}}$
10	276	100	11688.4	22896.0	45685.4	45368.9	45345.7	3.144	3.879
		150	27657.1	59634.0	120807.7	119423.1	119244.1		4.311
		200	43443.2	96156.0	195703.4	192967.8	192584.8		4.433
30	84	100		21927.0	42327.3	41755.9	41279.3	1.448	3.531
		150		56342.0	111871.5	109985.2	108361.5		3.918
		200		90394.0	181198.5	177870.8	174935.3		4.026
50	40	100			39287.1	38552.0	37789.8	1.128	3.233
		150			103724.0	101453.3	99075.1		3.582
		200			167950.6	163980.4	159823.7		3.679

two equal parts, as shown in Figure 11, the geometry becomes 4 elements and 23 nodes. The computer program was modified again to solve this case, using the same boundary conditions and assumptions as before. Results for this case are also tabulated in Tables 5 through 10.

C. DISCUSSION OF NUMERICAL RESULTS

Computer results for the finned copper condenser were generated for three outside convective coefficients, three fin angles and two rotation rates. The working fluid used throughout the analysis was water. Tables 5 through 10 compare the results of using 2, 3 and 4 elements, with those of Schafer [15].

Using the Finite Element solution, the heat transfer rates change less than 10 percent, as the number of elements change, so the heat transfer rates in the finned condenser can be approximated by 2 elements, and the error in the calculation of the heat transfer rates at the fin apex can be neglected. In comparing the smooth condenser to the finned condenser, the most dramatic improvement occurs for $\alpha = 50$ degrees with 40 fins. It is clear in this situation that $Q_{4 \text{ Element}}/Q_{\text{smooth}}$ is far greater than $A_{4 \text{ Element}}/A_{\text{smooth}}$.

The heat transfer rate was found to vary slightly with rotational speed in a finned condenser. This result agrees with the results obtained earlier by Schafer [15]. Schafer suggested that the invariance in heat transfer rate with

the rotation rate was due to the cancelling effects of decreasing film thickness and decreasing temperature difference across the film thickness as rotation rate is increased. The influence of external heat transfer coefficient, h_{out} , is shown in Tables 5 through 10. A large external heat transfer coefficient ($h_{out} = 5000$ BTU/hr-ft²-deg F) is seen to produce the largest heat transfer rates.

III. EXPERIMENTAL PROGRAM

A. EXPERIMENTAL EQUIPMENT

1. Description of Equipment

The equipment used to support the experimental program was the same equipment used by Loynes [18] and Wagenseil [19]. Figures 12 and 13 depict the experimental apparatus. The evaporator was a copper cylinder with O-ring seals at each end. Heat input to the evaporator was provided by a resistance heating element wrapped around the evaporator. The power supply for the heater element was changed from load bank resistors to a solid state phase amplifier power controller to reduce the space and inconvenience of the load banks. The model PA-1-2490 phase/amp is a single phase silicon controlled rectifier power amplifier designed to control and regulate A-C power. A six-volt battery was used as a power supply for the controller circuit.

The condenser was surrounded by a sealed insulated box. Garlock seals at each end of the condenser kept the cooling water from leaking out. The cooling water system, as shown schematically in Figure 14, was four supply tubes, 0.25 inch diameter with 0.031 inch holes drilled every 0.20 inch. The supply tubes ran the length of the condenser, parallel to the axis. Filtered and softened tap water was used as the cooling fluid. The inlet and outlet cooling

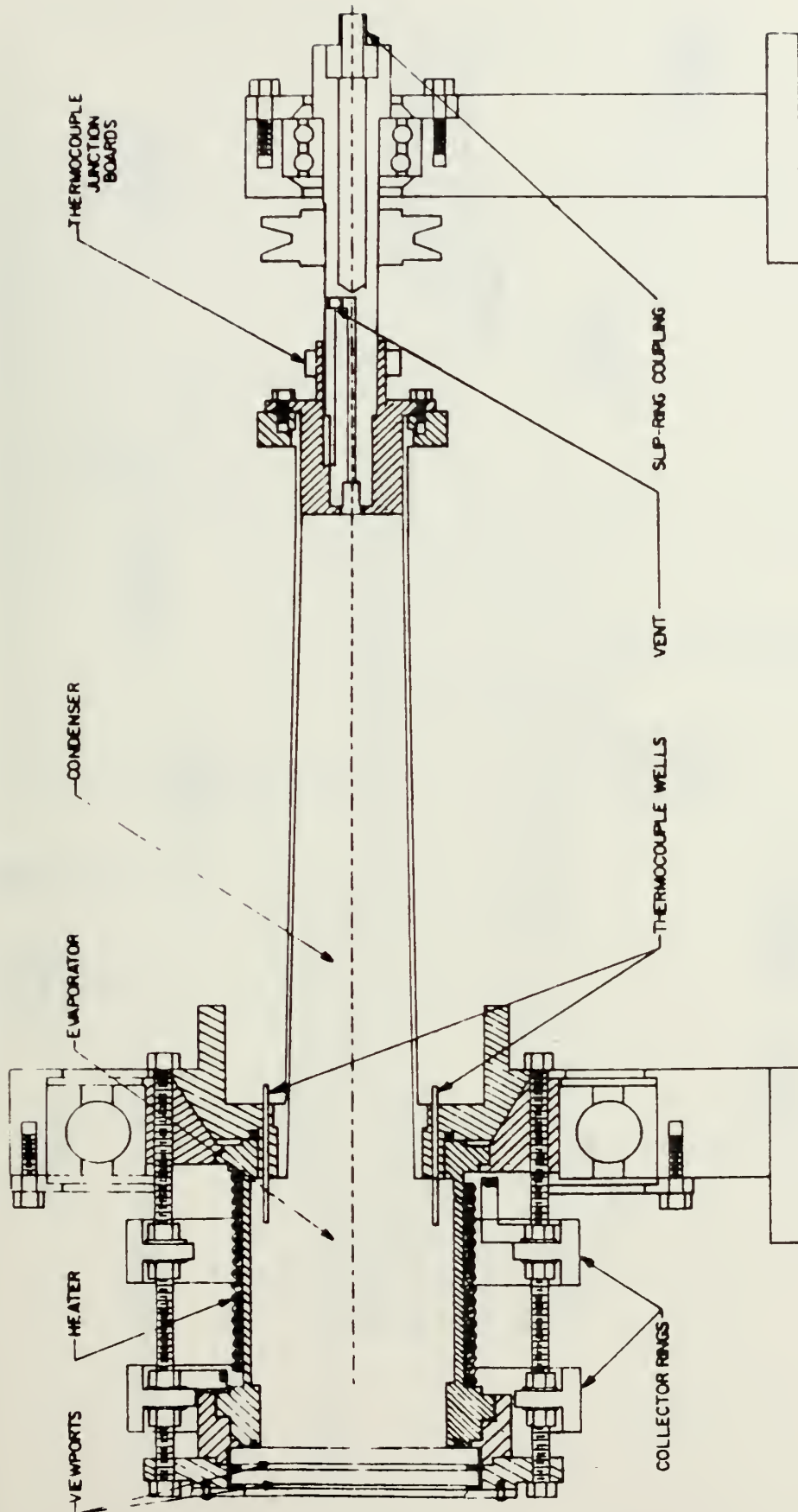


Figure 12. Cross Section of the Rotating Heat Pipe

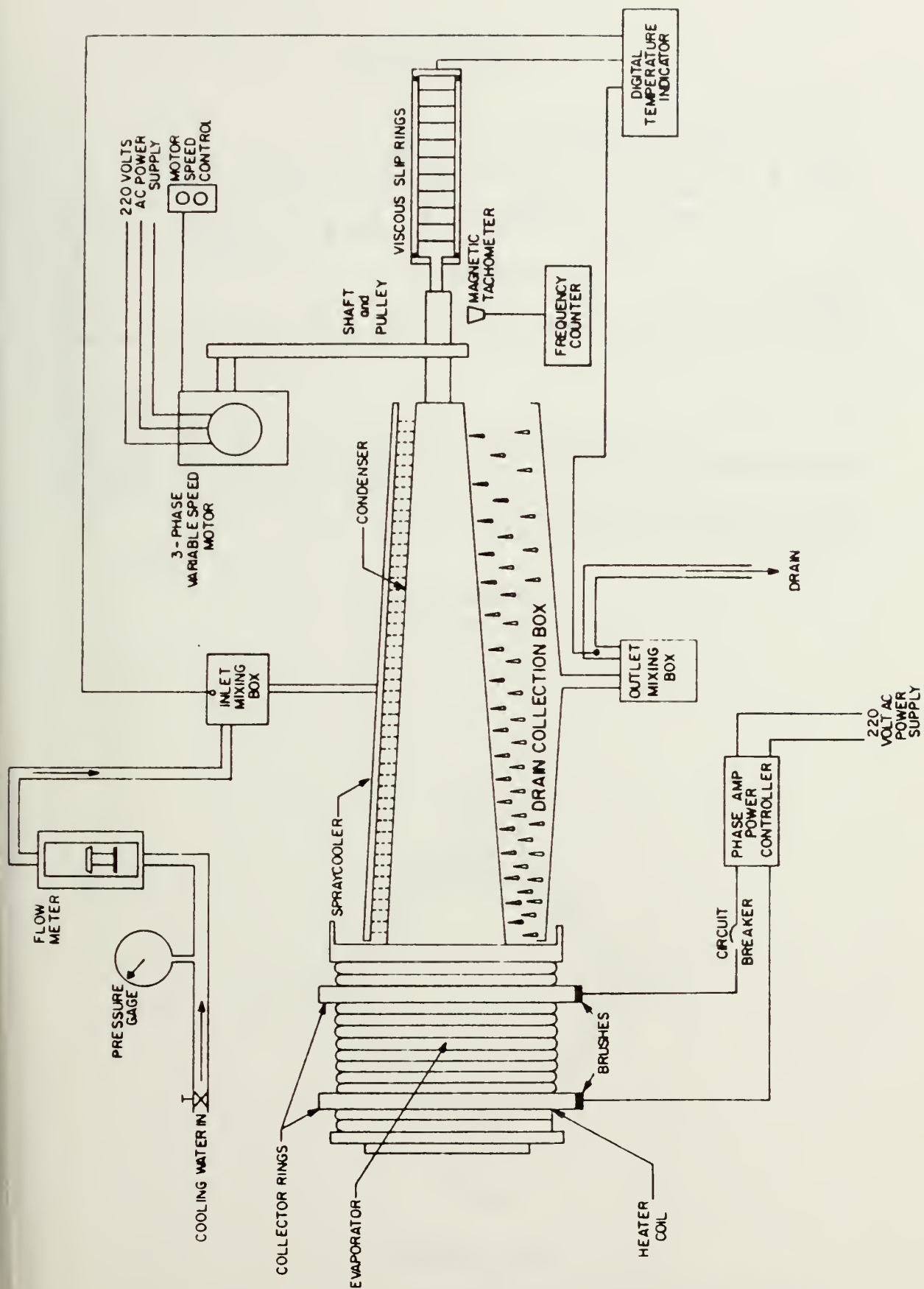
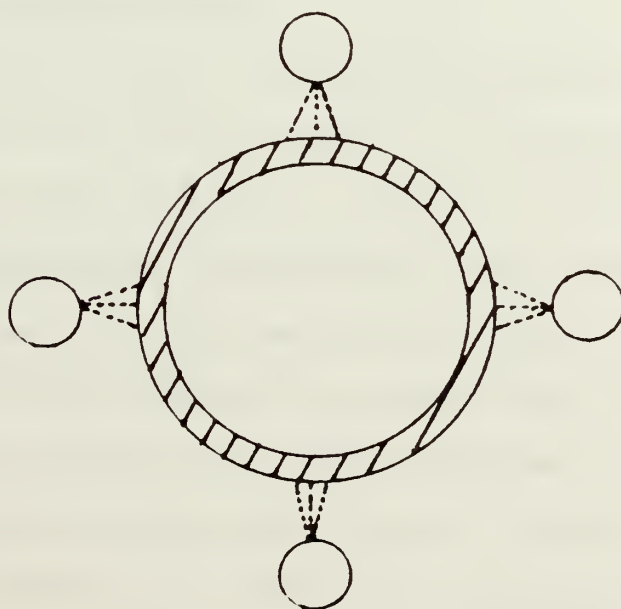
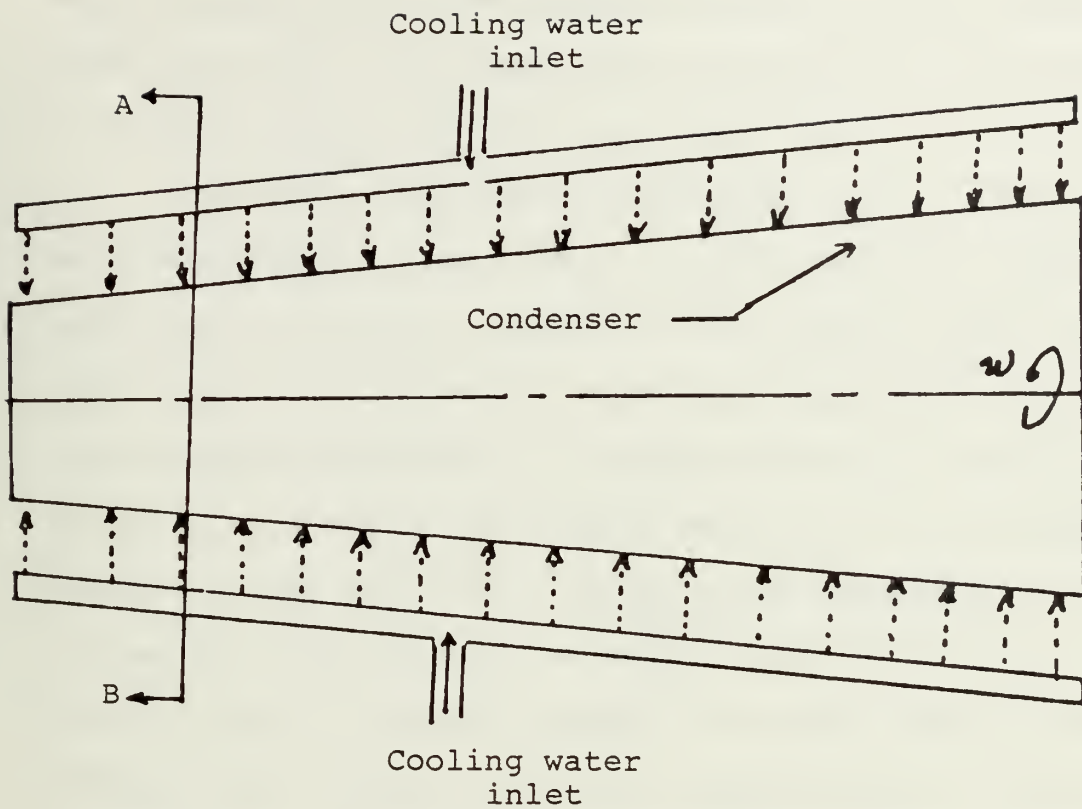


Figure 13. Schematic Diagram of Heat Pipe Apparatus



Section A-A

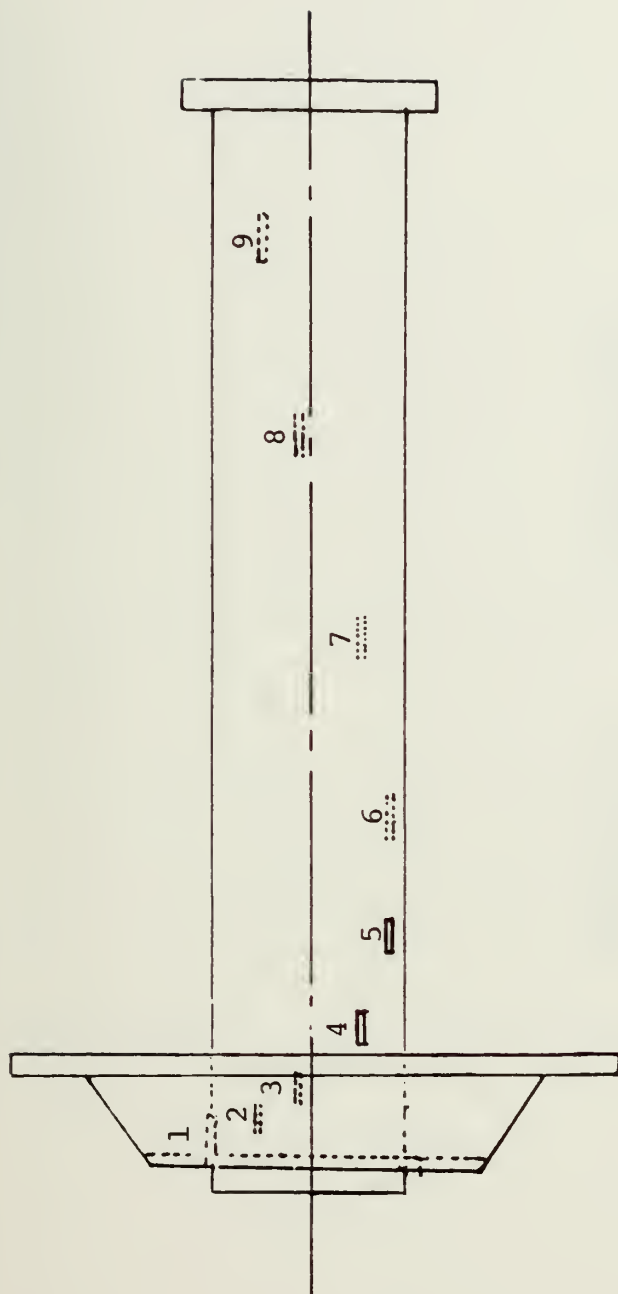
Figure 14. Impingement Cooling Schematic

water temperatures were measured along with the cooling water flow rate. The heat pipe was rotated in two bearings by a three phase variable speed motor with a V-belt drive.

A small drop-oiler was installed over the main bearing housing to lubricate the main bearing. This unit consisted of a small reservoir with a needle valve for flow regulation. A sight glass permitted observation of the oil flow from the reservoir to the main bearing. A flow rate of one drop every 20-30 seconds was found to be adequate. The end of the evaporator opposite the condenser contained a viewport consisting of two glass disks with an air space between them to prevent fogging. A strobe light shined through this viewport and, when synchronized to the rotational speed, allowed observation of the boiling action in the fluid annulus and the condensate in the condenser.

2. Instrumentation

The condenser wall was grooved out externally in nine places in Figures 15 and 16. The grooves were spaced 40 degrees apart and had a depth of 0.010 inch. Welded thermocouple beads were soldered into the grooves with a standard lead-tin low-temperature solder. The leads were secured to the condenser by banding with twisted wire and were passed through the small condenser flange to the mercury slip-ring unit on the test stand. Two additional thermocouples sheathed in 0.0625 inch stainless steel tubing penetrated the main flange. The sheathes protruded 2.0 inches



Thermocouple Number	Distance from Evaporator Wall, inches
1	0.100
2	0.250
3	0.750
4	1.050
5	2.000
6	3.000
7	5.050
8	7.000
9	9.050

Figure 15. Thermocouple Positions For 1.46 Inch Diameter and 1.00 Inch Diameter Cylinder

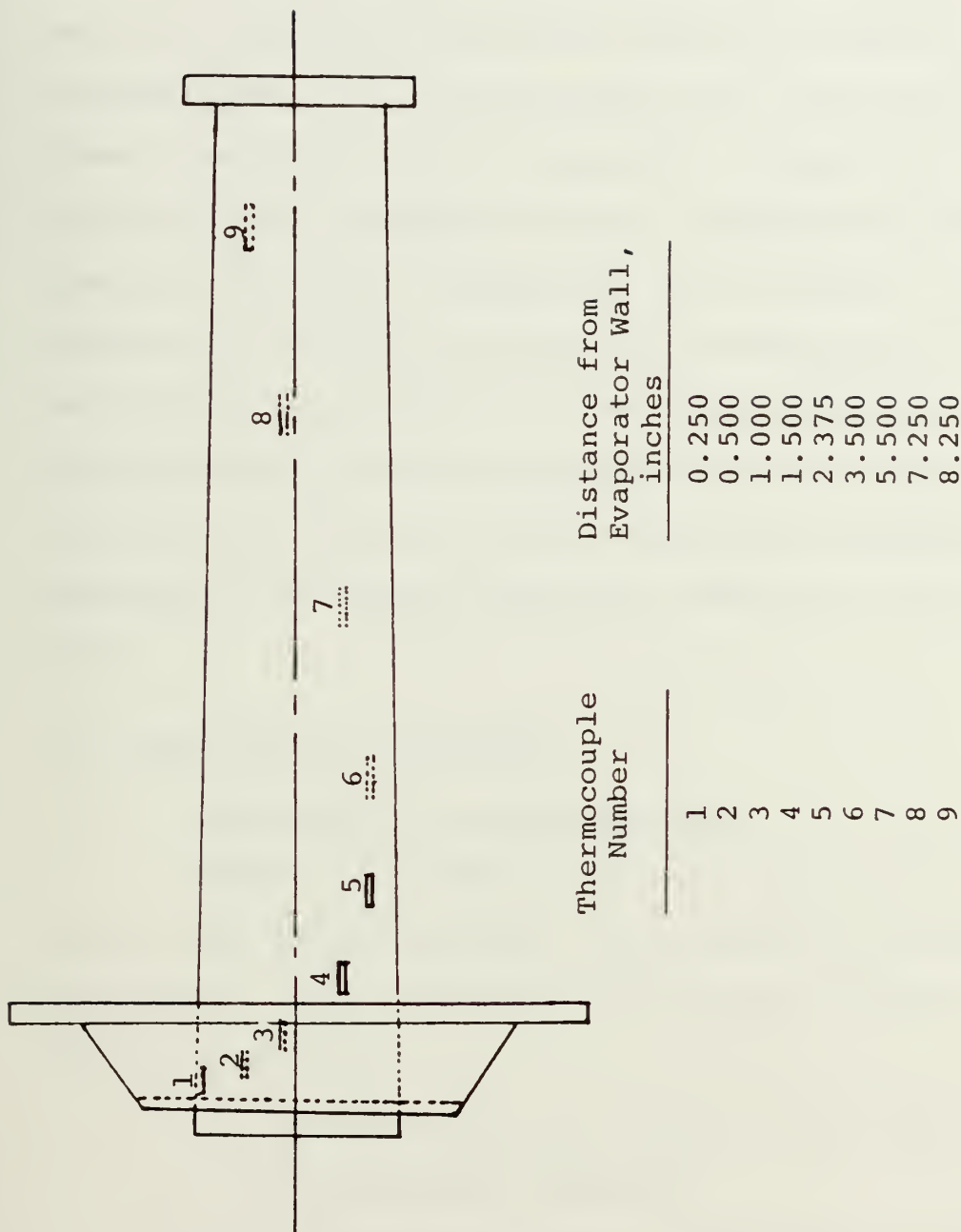


Figure 16. Thermocouple Positions For 0.5 Degree Cone

into the evaporator to measure the vapor temperature and were soldered closed at the tip to maintain the system vacuum. The inlet and outlet temperatures of the cooling water were monitored by Kapton insulated copper-constantan thermocouples. All thermocouples were read directly on a Newport Model 267 digital pyrometer. Calibration was performed in a Rosemount constant temperature bath using a platinum resistance thermometer as a standard. A graph of thermocouple error as a function of thermocouple reading was plotted to be used to correct each experimental reading. Cooling water flow rate was measured with a standard rotameter. Accurate regulation of the flow rate was accomplished by adjusting the pressure regulator installed in the cooling line.

B. EXPERIMENTAL PROCEDURES

1. Preparation of Condenser Wall

Tucker [20] established the procedure for preparation of the copper condenser for obtaining film condensation with water. This procedure was followed with the modifications listed below:

- a) The heat pipe was tilted so that the evaporator was depressed slightly.
- b) The standard cleaning steps were followed by scrubbing with a bristle brush. By depressing the evaporator end, cleaning fluids were prevented from running back into the heater assembly.

- c) Complete wetting of the condenser wall was observed after cleaning.

2. Filling and Venting Procedure

Instead of using the filling procedure of previous studies, a simpler procedure was used. The condenser was depressed, to nearly the vertical, with the evaporator end raised up. The heat pipe was then filled with about 350 ml of working fluid. The O-ring and glass viewports were installed. The bolts of the retainer ring were torqued to thirty inch-pounds in ten inch-pound steps to avoid cracking the glass window. This filling procedure was followed by a venting procedure, used by Tucker [20], with the modifications listed below:

- a) Tilt the heat pipe with the evaporator end down, until the working fluid covers up the viewport.
- b) Rotate the heat pipe by hand so that the vent screw is on top.
- c) Slowly apply the power to the heater to about 0.25 KW until the saturation temperature in the heat pipe is at least 220 degrees Fahrenheit for the distilled water.
- d) Back out the vent screw allowing some working fluid vapor to escape. Control the flow of the vapor with the vent screw, being careful to keep the pressure in the heat pipe above atmospheric pressure.

- e) Vent for a minimum of ten minutes for distilled water, to allow escaping steam to drive off air trapped within the system, leaving about 250 ml of working fluid left over.
- f) Turn off the electrical power and reseal the vent screw.
- g) Return the heat pipe to the horizontal position, and turn on the cooling water to the condenser.

3. Run Procedure

With filling and venting completed, the system was ready to be run. The standard run procedure was as follows:

- a) Open cooling water supply to the condenser and bearing cooling water lines.
- b) Start the cooling water supply pump, and adjust the rotameter to the desired flow rate. In this experiment, only the 50 percent flow rate was used.
- c) Oil the evaporator bearing.
- d) Energize and start the drive motor. Increase the speed to 1100 RPM to insure an annulus has formed in the evaporator.
- e) Set rotational speed to the desired value.
- f) Let the system reach steady state; take zero power thermocouple, cooling water flow rate and tachometer readings.
- g) Set power to heater to desired level and allow the system to come to steady state. Take

tachometer, cooling water flow rate, thermocouple, voltage and ampere readings.

- h) Repeat step g) for each power level desired.
- i) Repeat step f).
- j) Repeat steps e) through i) for each rotational speed desired.

4. Data Reduction

Data were reduced by correcting the recorded thermocouple readings to obtain a true reading in degrees Celsius. Correction was accomplished using thermocouple calibration curves. The Celsius readings were then converted to degrees Fahrenheit. Percentage flow rate was converted to pounds per hour using the rotameter calibration curve. Heat transfer for each run was calculated as the product of the cooling water mass flow rate, the difference in temperature between cooling water outlet and inlet and the specific heat of the cooling water using the basic equation:

$$\dot{Q} = \dot{m} C_p \Delta T \quad (40)$$

where

\dot{m} = cooling water mass flow rate, lbm/hr

C_p = specific heat of the cooling water, taken as one BTU/lbm-deg F

ΔT = the temperature difference between the cooling water outlet and inlet, deg F.

To correct for heat generated by friction in the Garlock seals and by viscous dissipation of the cooling water, the average zero power heat transfer rate was subtracted from the measured heat transfer rate in order to give a corrected heat transfer rate.

IV. DISCUSSION OF EXPERIMENTAL RESULTS

A. EXPERIMENTAL RESULTS

The various experimental runs are shown in Table 11. All the heat pipes in this thesis were run at 700, 1400 and 2800 RPM, except the 1.00 inch diameter cylindrical condenser which was run at 1800 and 2800 RPM for the fourth run and 1400 and 2800 RPM for the fifth run due to erratic readings of most of the thermocouples at the low rotation speed. It was concluded that the problem existed in the slip-ring unit and was due to dirty mercury in the slip-ring. So after the fifth run, the slip-ring unit was cleaned by taking the mercury and using methanol to clean the inside. Nitrogen was blown into the unit to dry it out. New mercury was added prior to the sixth run. The plots of heat transfer rate versus saturation temperature are referred to as the performance curves.

Figures 17, 18, and 19 show the results of different condensers. In all cases, the heat transfer rate increased with increasing RPM. In the cases of the rotating cylindrical condenser, the condensate flow is induced not by centrifugal force but by a hydrostatic pressure gradient established in the condensate as a result of its variable film thickness. By increasing the diameter of the cylinder from 1.00 inch to 1.46 inches, the heat transfer capacity increases. For the 0.5 degree truncated cone, the heat transfer is higher

TABLE 11
Summary of Experimental Runs

Run No.	Geometry	RPM	Test Fluid
1	Cylindrical 1.46 inch diameter	700 1400 2800	Water
2	Cylindrical 1.46 inch diameter	700 1400 2800	Freon 113
3	Cylindrical 1.46 inch diameter	700 1400 2800	Ethanol
4	Cylindrical 1.00 inch diameter	1800 2800	Water
5	Cylindrical 1.00 inch diameter	1400 2800	Water
6	0.5 degree trun- cated cone	700 1400 2800	Water
7	0.5 degree trun- cated cone	700 1400 2800	Water

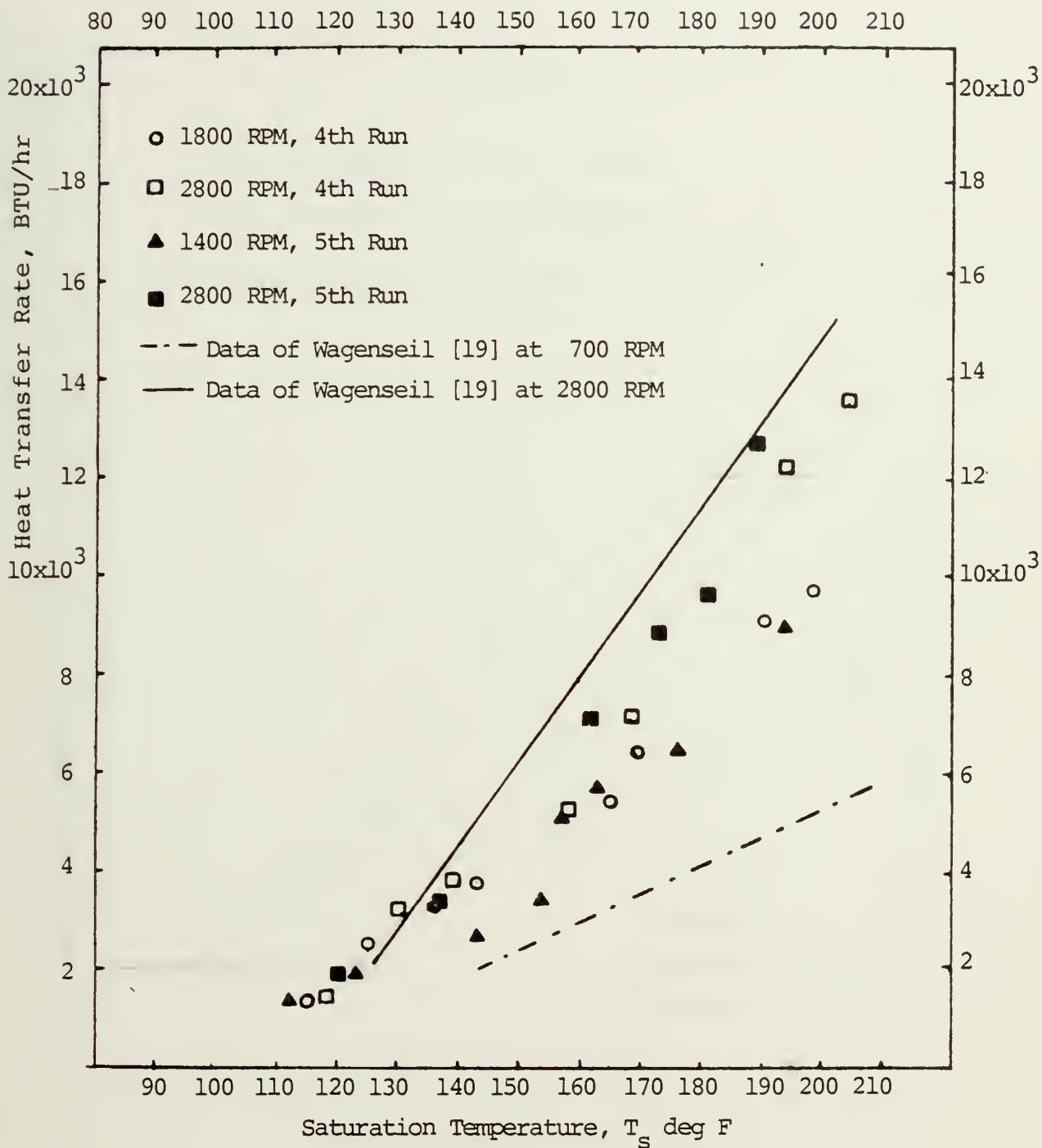


Figure 17. Heat Transfer Rate Versus Saturation Temperature for Cylindrical 1.00 Inch Diameter Condenser

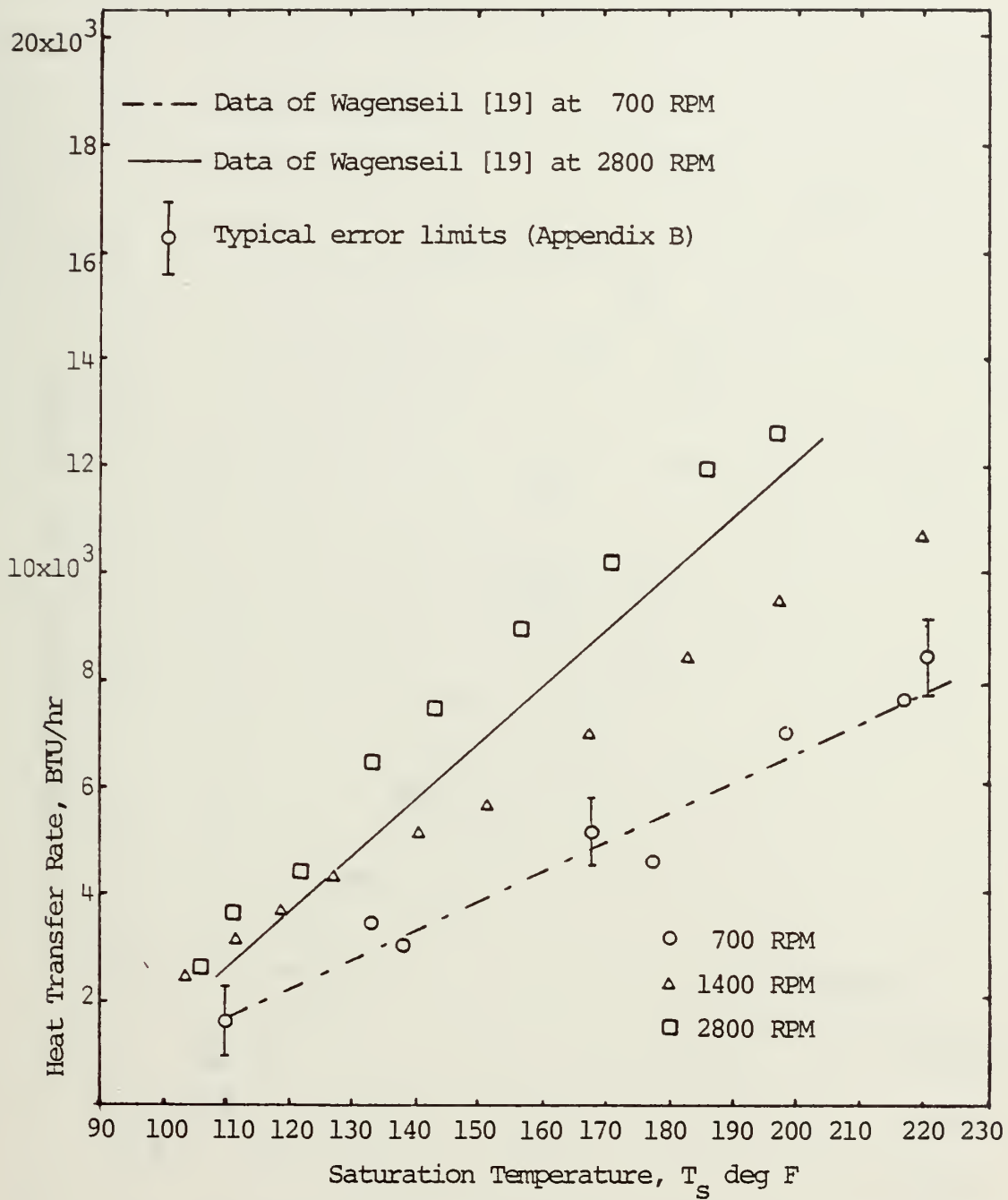


Figure 18. Heat Transfer Rate Versus Saturation Temperature for Cylindrical 1.46 Inch Diameter Condenser

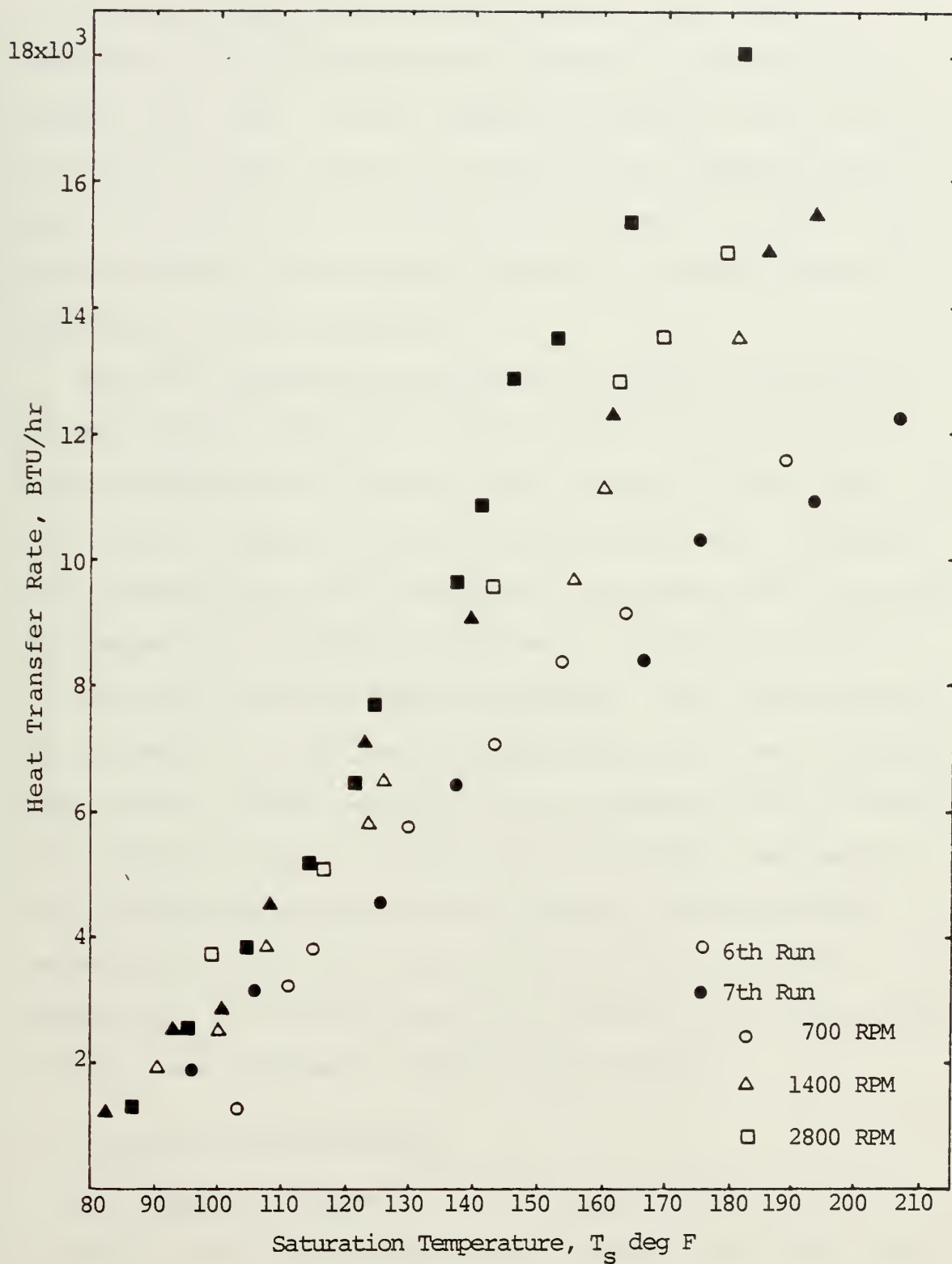


Figure 19. Heat Transfer Rate Versus Saturation Temperature for Truncated Cone Condenser with 0.5 Degree Half Angle

than the cylindrical condenser. This improvement is due to the centrifugal force which increases the axial force component on the condensate and thereby increases the condensate flow rate. This increase in working fluid circulation simply means that more vapor can be condensed per unit time. The increase in centrifugal force also flattens the condensate film and thereby reduces the overall thermal resistance in the condenser.

The wall temperature profiles as shown in Figures 20, 21 and 22 were taken from the 1.46 inch diameter cylindrical condenser at different RPM. Figure 23 was taken from the 0.5 degree truncated cone at 700 RPM. Distance zero corresponds to the condenser end nearest the evaporator. The temperatures would be expected to be nearly constant if the heat pipe were truly isothermal. For the cylindrical condenser, the highest temperature is at the evaporator end, and the lowest temperature is at about 0.25 inch from the evaporator end. For the truncated cone, the temperature profile decreases almost linearly, and the highest temperature is at the evaporator end. This increase in temperature at the evaporator is probably due to conduction effects from the heater and the main bearing.

B. ANALYSIS OF THE RESULTS

To compare the theoretical and experimental results, a log-log plot of the mean Nusselt number versus the Sherwood number was made. To make this comparison of theoretical

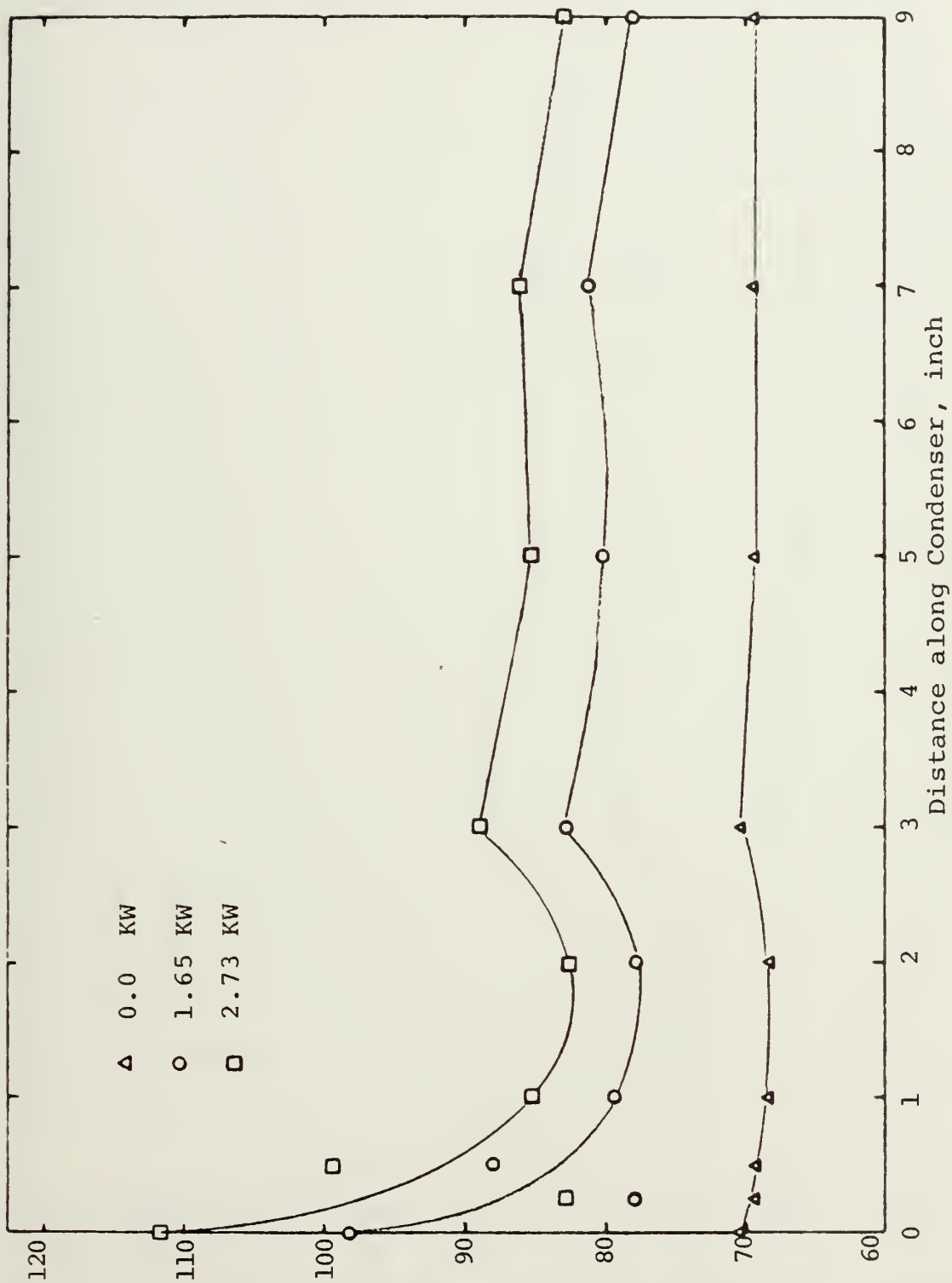


Figure 20. Condenser Outside Surface Temperature Profile at 700 RPM for 1.46 Inch Diameter Cylindrical Condenser

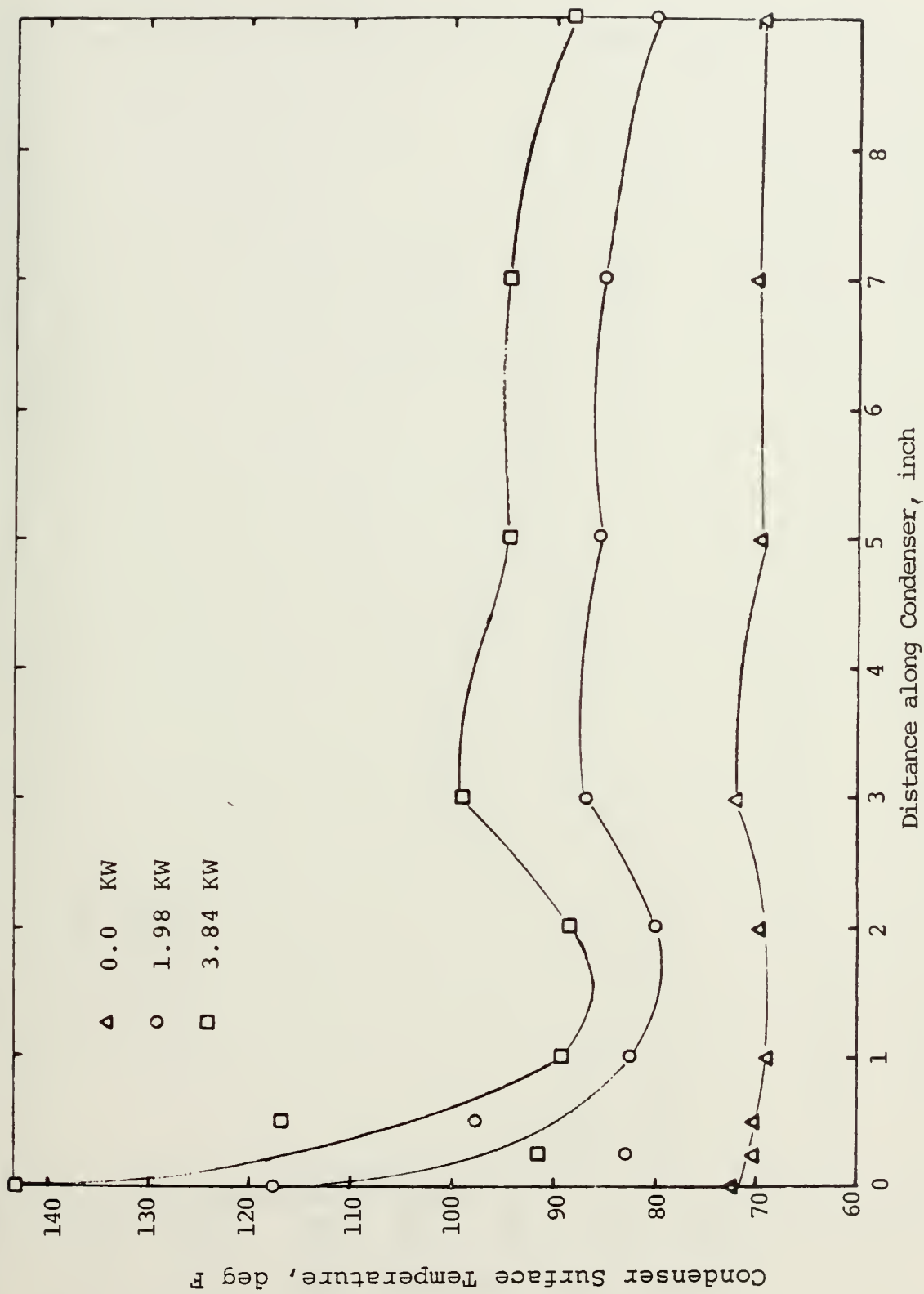


Figure 21. Condenser Outside Surface Temperature at 1400 RPM for 1.46 Inch Diameter Cylindrical Condenser

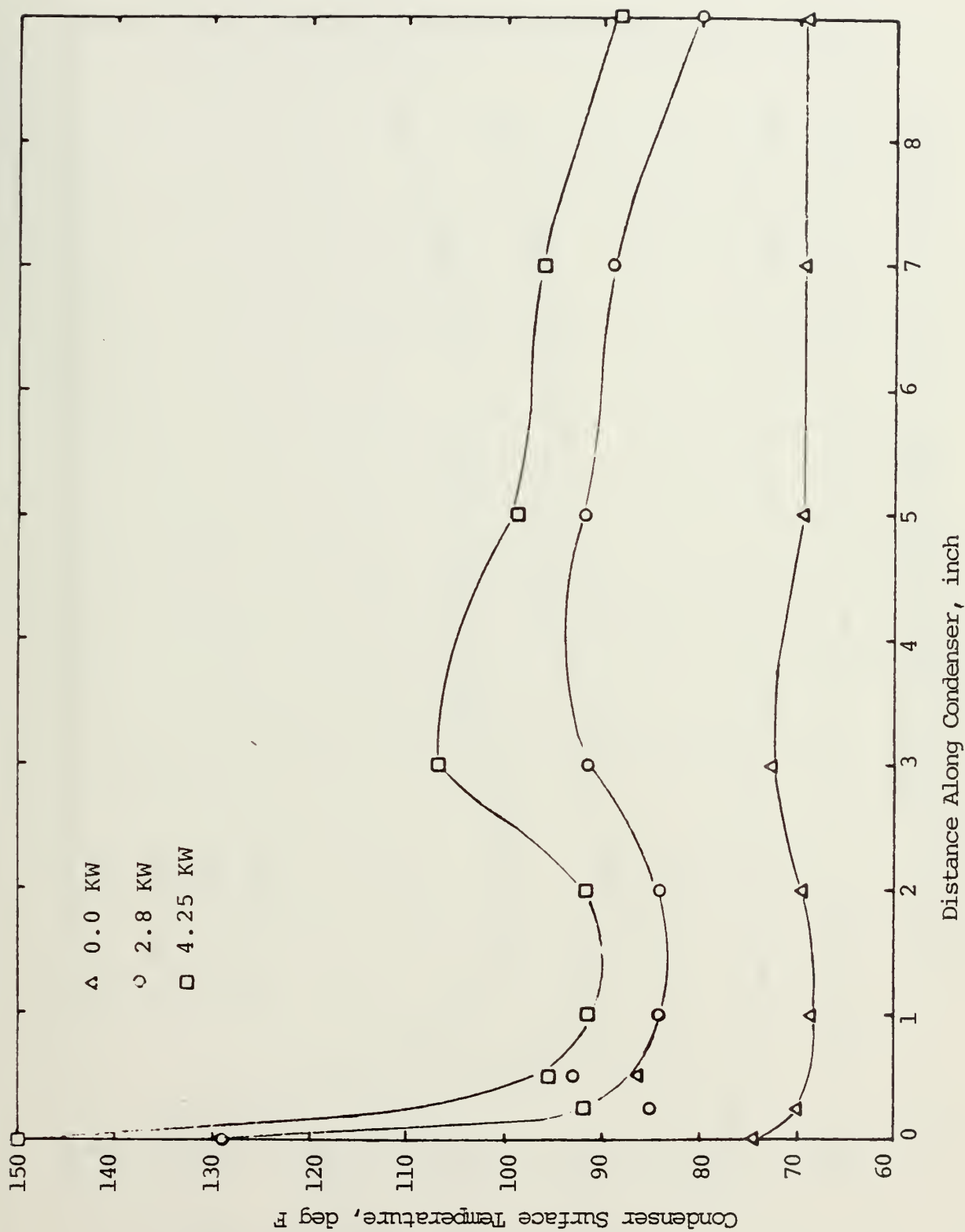


Figure 22. Condenser Outside Surface Temperature Profile at 2800 RPM for 1.46 Inch Diameter Cylindrical Condenser

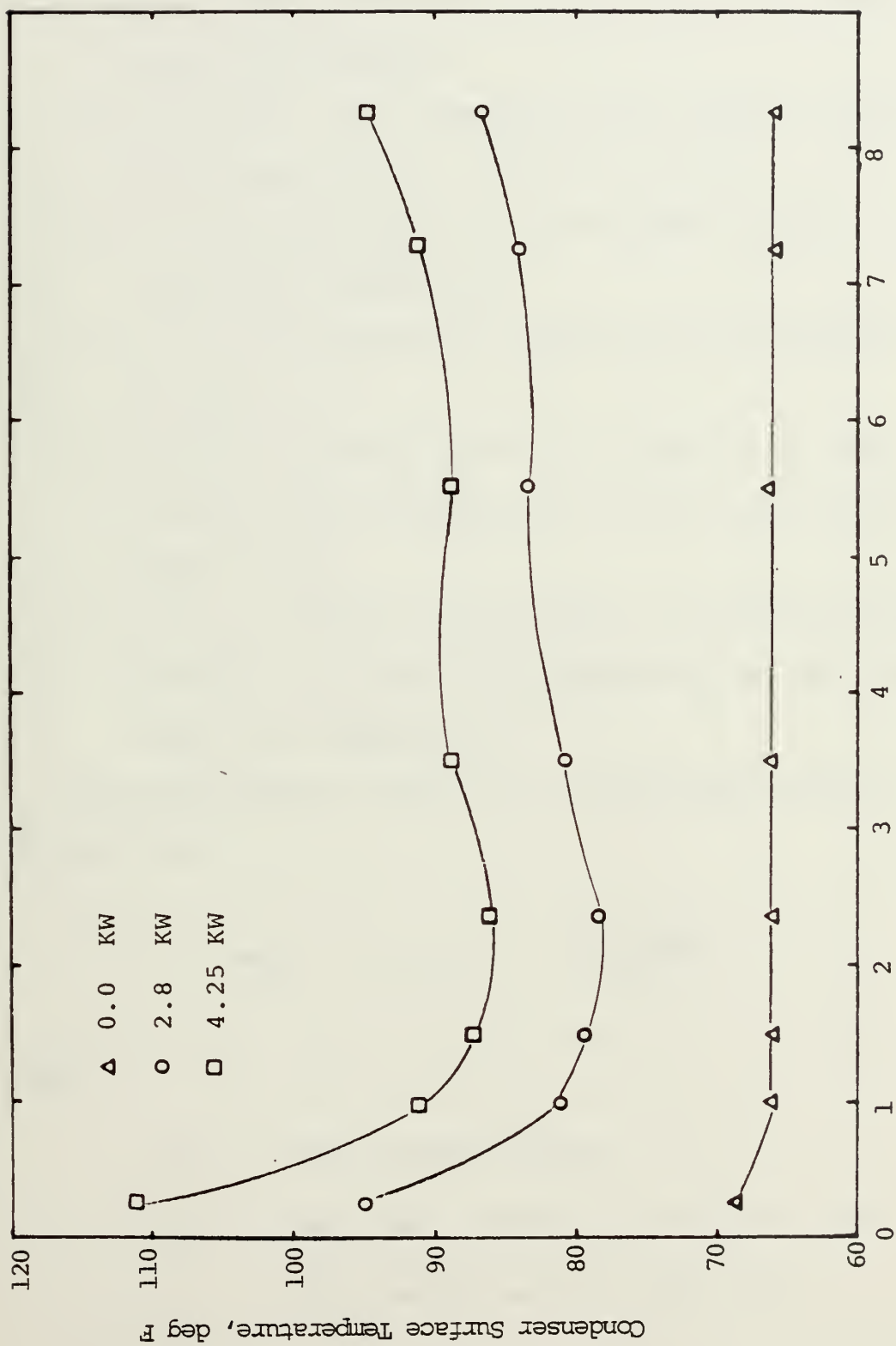


Figure 23. Condenser Outside Surface Temperature Profile at 700 RPM for 0.5 Degree Truncated Cone

versus experimental results, the following simplifications were made:

- 1) The thermal conductivity of the wall was constant along the condenser,
- 2) the inside wall temperature was found by using a direct application of Fourier's law,
- 3) all fluid properties were evaluated at the saturation temperature,
- 4) heat flux through the condenser was considered uniform,
- 5) for the truncated cone, the surface area used the average radius between the entrance and the exit radius, and
- 6) for $h_m = Q/A\Delta T$, ΔT was taken as the difference between the saturation temperature and the condenser inner wall temperature.

The mean Nusselt number for a given heat transfer rate is given by:

$$Nu_m = h_m L/k = \frac{(Q/A \Delta T) L}{k} \quad (41)$$

where

Nu_m = mean Nusselt number

h_m = mean heat transfer coefficient, BTU/hr-ft²-deg F

A = the average surface area, ft²

k = thermal conductivity of the fluid,
BTU/hr-ft-deg F

L = condenser length, ft

The mean Nusselt number was determined from the data, and this value was plotted against the corresponding Sherwood number. Figure 24 shows Nu_m versus Sherwood number for the cylindrical condensers. For water with the 1.46 inch diameter cylindrical condenser, the experimental data agree with equation (11). The data using the 1.00 inch diameter cylindrical condenser, however, show that the Nu_m increases with decreasing Sh . This trend is the opposite to what was expected. The reason for this trend may be due to: (1) ripples in the condensate film due to higher vapor velocities or (2) a high uncertainty in the low power runs. For Freon 113 and ethanol, with the 1.46 inch diameter cylindrical condenser, the experimental results are higher than but are parallel to equation (11). The reason for this discrepancy is not clear at this time. It may be due to differences in vapor densities between water, Freon 113 and ethanol, leading to differences in non-condensable gas migration, or to differences in vapor velocity effects within the theoretical model.

Figure 25 shows the mean Nusselt number versus the Sherwood number of the truncated cone to find out the best correlation between the theoretical and experimental results. The results of Dhir and Lienhard [8], and Roetzel [14] were

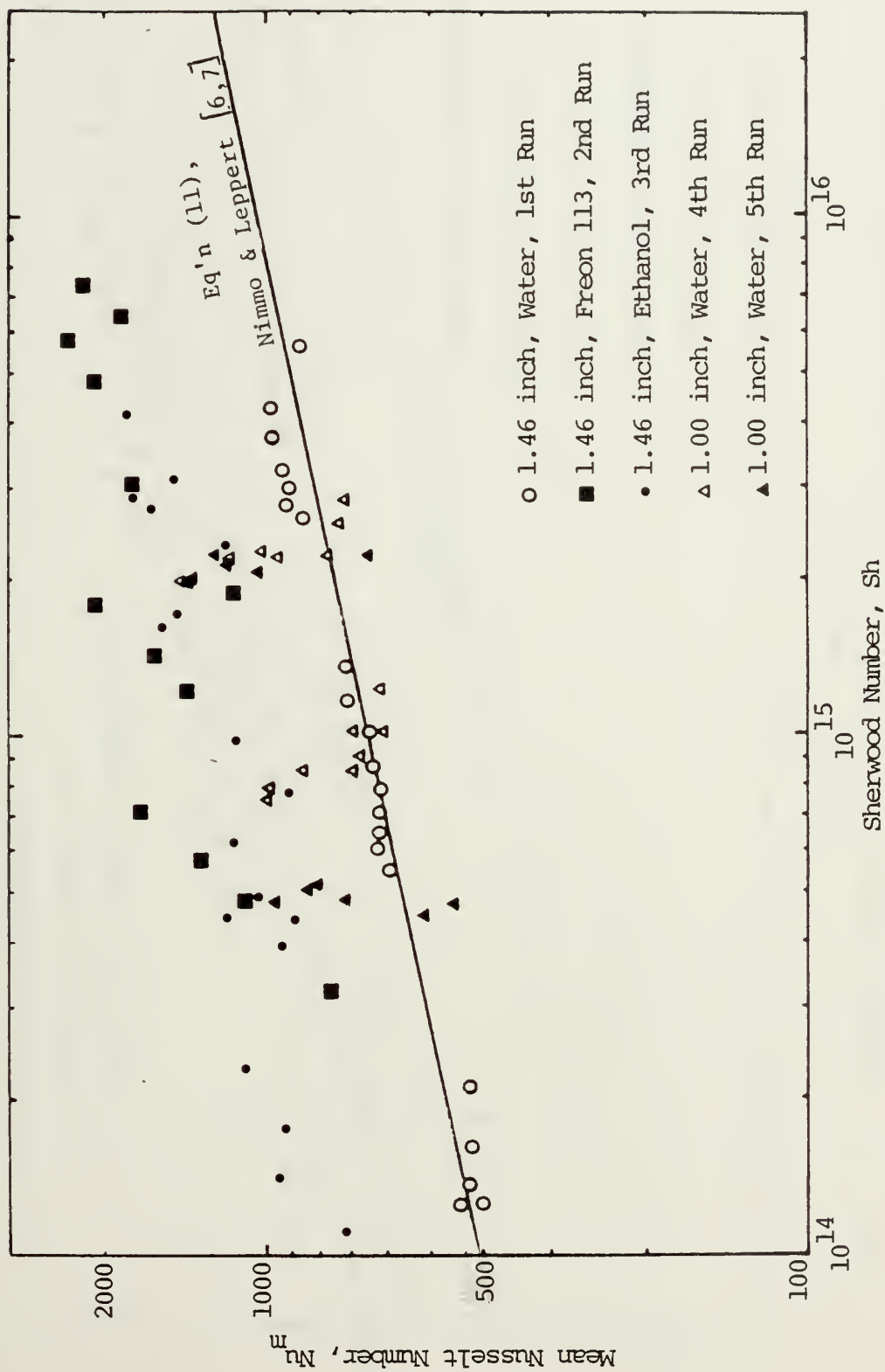


Figure 24. Nusselt Number Versus Sherwood Number for Cylindrical Condensers

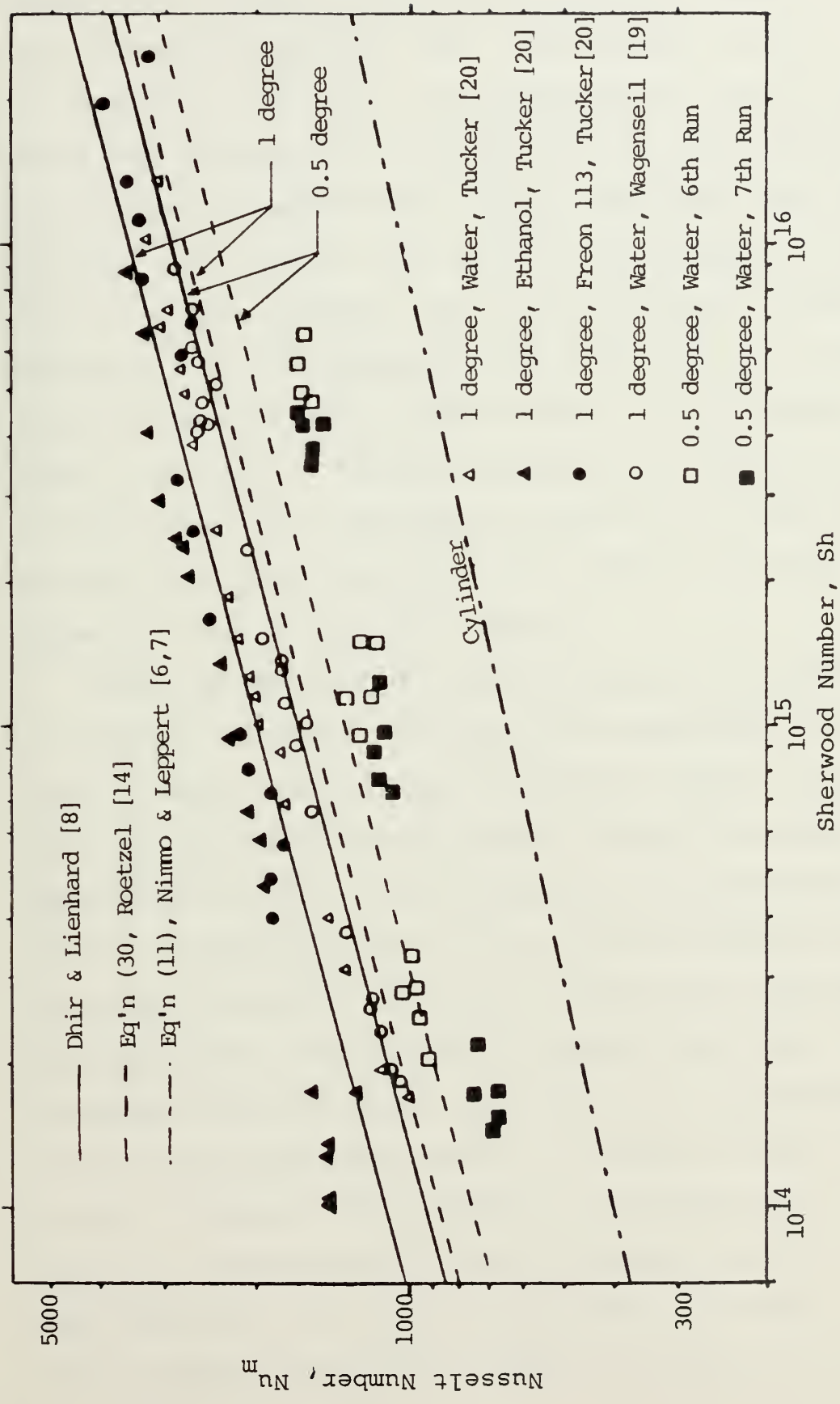


Figure 25. Nusselt Number Versus Sherwood Number for Truncated Cone Condensers

chosen to be compared with the experimental results. For the one degree truncated cone, using Tucker's data [20] and Wagenseil's data [19], the experimental results for water fall between both analyses, whereas for ethanol and Freon 113, the experimental results are higher than both analyses. This may be due again to differences in vapor densities between water, Freon 113 and ethanol, leading to differences in non-condensable gas migration, or to differences in vapor velocity effects within the theoretical model. For the 0.5 degree truncated cone with water as the working fluid, the experimental results fall lower than both analyses, but fall higher than the analysis of Nimmo and Leppert [7] for a straight cylinder.

Figure 26 shows Nu_m/Nu_∞ plotted versus the parameters of Roetzel's analysis. By using all experimental results taken to data at the Naval Postgraduate School, it appears that good agreement exists between Roetzel's analysis and experimental results. The differences of experimental results and Roetzel's for the cylindrical condensers are less than 15 percent. For the truncated cone condensers, the differences are less than 20 percent for water. For the truncated cone with ethanol and Freon 113, experimental results are higher than Roetzel's analysis by about 35 percent. However, the agreement is reasonable and the analysis of Roetzel can be used to predict rotating heat pipe performance to within ± 20 percent for water. For Freon 113 and ethanol the data lies above the theory by +35 percent.

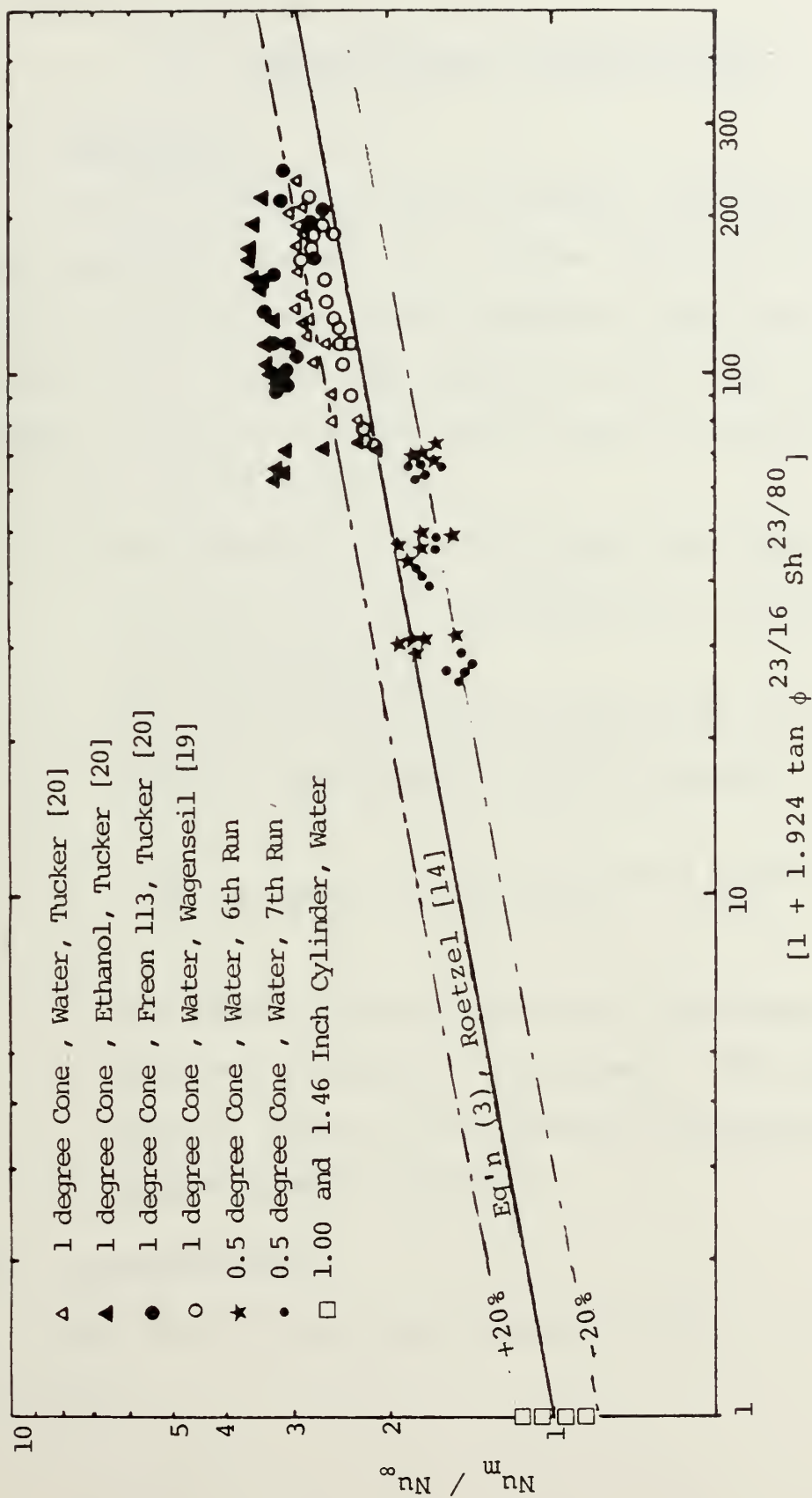


Figure 26. Comparison of Experimental Data with Theory of Roetzel [14]

V. CONCLUSIONS AND RECOMMENDATIONS

A. CONCLUSIONS

For an internally finned condenser, the analysis of the condenser heat transfer problem using a two-dimensional wall conduction model and a parabolic temperature distribution along the fin can be approximated by the two-element Finite Element solution with twenty-five axial increments.

For a smooth condenser:

1. The theoretical work of Leppert and Nimmo [6,7] can be used to predict satisfactorily cylindrical heat pipe performance.
2. The theoretical equation which best predicts overall heat pipe performance is due to Roetzel [14]:

$$Nu_m = Nu_{\infty} [1 + 1.924 \tan \phi^{23/16} Sh^{23/80}]^{4/23} .$$

The above equation agrees with the experimental data of water to within ± 20 percent. The experimental data of Freon 113 and ethanol lie approximately 35 percent above the theory.

B. RECOMMENDATIONS

Continue to study the internally finned, rotating heat pipe by:

1. Re-examining the Finite Element analysis using the mirror geometry presented in Figure 7.
2. Analyzing film condensation on a variety of fin shapes, and applying the solution of the two-dimensional model to determine the shape permitting optimum heat transfer rate.
3. Manufacturing an internally finned condenser to obtain experimental data to compare with the theoretical analysis.

Continue to study the smooth, rotating heat pipe by:

1. Using a condenser section with a half cone angle greater than 1 degree to obtain additional experimental data to compare to Roetzel's analysis.
2. Examining reasons why the Freon 113 and ethanol data are falling above the theory.

APPENDIX A

CALIBRATION OF MEASUREMENT DEVICES

1. Calibration of the Thermocouples

The thermocouples for both the cylindrical and the truncated cone were calibrated, after they had been soldered to the outside condenser wall, in a ROSEMOUNT variable temperature oil bath utilizing a platinum resistance thermometer as the standard of measurement. They were calibrated in five degree increments, from 10 to 90 degrees Celsius. Each thermocouple was wired to a channel on the Newport Model 267 Digital Pyrometer giving individual readings in degrees Celsius. For each thermocouple the difference $T_{act} - T_i$ was calculated where:

T_{act} = reading in degrees Celsius of the standard,
and

T_i = reading in degrees Celsius for the i^{th}
thermocouple at the same temperature.

The mean of these differences was determined and used as the data point for plotting, $T_{act} - T_{recorded}$, versus thermocouple reading in degrees Celsius at known temperature. The maximum difference between the mean reading and each individual reading was one degree Celsius.

2. Calibration of the Rotameter

The cooling water flow rotameter was calibrated using a Toledo scale, a large container and an electric

timer. Calibration proceeded in 5 percent flow increments from 15 to 90 percent flow rate. Water was collected for as long as 300 seconds at the lower flow rates and for a minimum of 140 seconds at the maximum flow rate. Each flow rate was measured two times. The flow rate (lbm/hr) was plotted versus percentage flow through the rotameter. This curve was used to determine mass flow rate.

APPENDIX B
UNCERTAINTY ANALYSIS

The method of Kline and McClintock [21] was used to estimate the uncertainties in the experimental heat transfer rate. The heat transfer of the heat pipe is given by:

$$Q_{\text{total}} = Q_t = \dot{m} C_p \Delta T_t$$

$$Q_{\text{frictional loss}} = Q_f = \dot{m} C_p \Delta T_f$$

$$Q_{\text{corrected}} = Q_t - Q_f$$

where

Q_t = total heat transferred to cooling water, BTU/hr

Q_f = heat transferred to cooling water due to friction, BTU/hr

Q_c = corrected heat transfer rate, BTU/hr

\dot{m} = mass flow rate of cooling water, lbm/hr

C_p = specific heat of cooling water, BTU/lbm-deg F

ΔT_t = difference of cooling water outlet and inlet temperatures, deg F

ΔT_f = difference of cooling water outlet and inlet temperatures due to heat of friction, deg F

The uncertainties of these quantities are designated:

$$W_Q, \dot{W}_m, W_{C_p} \text{ and } W_{\Delta T}$$

The fractional uncertainties are given by

$$\frac{W_{Q_f}}{Q_f} = \left(\left(\frac{\dot{W}_m}{\dot{m}} \right)^2 + \left(\frac{W_{C_p}}{C_p} \right)^2 + \left(\frac{W_{\Delta T_f}}{\Delta T_f} \right)^2 \right)^{1/2} \quad (\text{B-1})$$

$$\frac{W_{Q_t}}{Q_t} = \left(\left(\frac{\dot{W}_m}{\dot{m}} \right)^2 + \left(\frac{W_{C_p}}{C_p} \right)^2 + \left(\frac{W_{\Delta T_t}}{\Delta T_t} \right)^2 \right)^{1/2} \quad (\text{B-2})$$

The uncertainty for the corrected heat transfer rate is given by:

$$W_{Q_c} = \left(W_{Q_t}^2 + W_{Q_f}^2 \right)^{1/2} \quad (\text{B-3})$$

The values and uncertainties of the measured quantities were taken to be:

$$C_p = 1.000 \text{ BTU/lbm-deg F}$$

$$W_{C_p} = \pm 0.002 \text{ BTU/lbm-deg F}$$

$$\dot{m} = 50 \text{ percent of maximum flow rate} = 1790 \text{ lbm/hr}$$

$$\dot{W}_m = \pm 1 \text{ percent}$$

$$W_{T_{in}}, W_{T_{out}} = \pm 0.18 \text{ deg F}$$

$$W_{\Delta T} = \left(W_{T_{in}}^2 + W_{T_{out}}^2 \right)^{1/2}$$

Using the 1.460 inch diameter cylindrical condenser run
at 700 RPM, the uncertainty limits are:

T_s (deg f)	Q_c (BTU/hr)	UNCERTAINTY, W_{Q_c}	
110.6	1611.0	± 634.6	$\pm 39.4\%$
133.8	3222.0	± 637.7	$\pm 19.8\%$
138.2	3222.0	± 641.4	$\pm 19.9\%$
168.4	5155.2	± 643.6	$\pm 12.5\%$
198.1	7088.4	± 651.8	$\pm 9.2\%$
218.9	7732.8	± 655.0	$\pm 8.5\%$
222.8	8377.2	± 658.4	$\pm 7.8\%$

BIBLIOGRAPHY

1. Ballback, L. J., The Operation of a Rotating Wickless Heat Pipe, M. S. Thesis, Naval Postgraduate School, Monterey, California, December 1969.
2. Kutateladze, S. C., "On the Transition to Film Boiling Under Natural Convection," Kotloturbostroenie, No. 3, pp. 10, 1948.
3. Sakhuja, R. K., "Flooding Constraint in Wickless Heat Pipes," ASME Paper No. 73-WA/HT-7.
4. Sparrow, E. M., and Gregg, J. L., "A Theory of Rotating Condensation," Journal of Heat Transfer, Vol. 81, Series C, pp. 113-120, May 1959.
5. Sparrow, E. M., and Hartnett, J. P., "Condensation on a Rotating Cone," Journal of Heat Transfer, Vol. 83, Series C, No. 1, pp. 101-102, February 1961.
6. Leppert, G., and Nimmo, B. G., "Laminar Film Condensation on Surfaces Normal to Body or Inertial Forces," Transactions of the ASME, p. 178, February 1968.
7. Nimmo, B. G., and Leppert, G., Laminar Film Condensation on Finite Horizontal Surface, Clarkson College of Technology, Potsdam, New York, 1970.
8. Dhir, V., and Lienhard, J., "Laminar Film Condensation of Plane and Axisymmetric Bodies in Nonuniform Gravity," Journal of Heat Transfer, Trans. ASME, Series C, Vol. 93, No. 1, Feb 1971, p. 97-100.
9. Daley, T. J., The Experimental Design and Operation of a Rotating, Wickless Heat Pipe, M. S. Thesis, Naval Postgraduate School, Monterey, California, June 1970.
10. Newton, W. H., Performance Characteristics of Rotating, Non-Capillary Heat Pipes, M. S. Thesis, Naval Postgraduate School, Monterey, California, June 1971.
11. Daniels, T. C., and Al-Jumaily, F. K., Theoretical and Experimental Analysis of a Rotating, Wickless Heat Pipe, Proceedings of the 1st International Heat Pipe Conference, Stuttgart, 1973.

12. Daniels, T. C., and Al-Jumaily, F. K., Investigations of the Factors Affecting the Performance of a Rotating Heat Pipe, International Journal of Heat and Mass Transfer, Vol. 18, p. 961, 1975.
13. Marto, P. J., Performance Characteristics of Rotating, Wickless Heat Pipes, Proceedings of the 2nd International Heat Pipe Conference, p. 281-291, Bologna, Italy 1976.
14. Roetzel, W., "Improving Heat Transfer in Steam Heated Fast Rotating Paper Drying Drums," International Journal of Heat and Mass Transfer, Vol. 18, p. 79-86, 1975.
15. Schafer, C. E., Augmenting the Heat Transfer Performance of Rotating, Two-Phase Thermosyphons, M. S. Thesis, Naval Postgraduate School, Monterey, California, December 1972.
16. Corley, R. D., Heat Transfer Analysis of a Rotating Heat Pipe Containing Internal Axial Fins, M. S. Thesis, Naval Postgraduate School, Monterey, California, June 1976.
17. Lew, G. T., A Three-Dimensional Solution of the Transient Field Problem Using Isoparametric Finite Elements, M. S. Thesis, Naval Postgraduate School, Monterey, California, December 1972.
18. Loynes, J. L., Design Improvements on a Rotating Heat Pipe Apparatus, M. S. Thesis, Naval Postgraduate School, Monterey, California, September 1976.
19. Wagenseil, L. L., Heat Transfer Performance of Various Rotating Heat Pipes, M. S. Thesis, Naval Postgraduate School, Monterey, California, December 1976.
20. Tucker, R. S., Heat Transfer Characteristics of a Rotating Two-Phase Thermosyphon, M. S. Thesis, Naval Postgraduate School, Monterey, California, September 1974.
21. Kline, S. J., and McClintock, F. A., "Describing Uncertainties in Single-Sample Experiments," Mechanical Engineering, p. 3, January 1953.

INITIAL DISTRIBUTION LIST

	No. Copies
1. Defense Documentation Center Cameron Station Alexandria, Virginia 22314	2
2. Library, Code 0142 Naval Postgraduate School Monterey, California 93940	2
3. Department of Mechanical Engineering Code 69 Naval Postgraduate School Monterey, California 93940	1
4. Dr. P. J. Marto, Code 69Mx Department of Mechanical Engineering Naval Postgraduate School Monterey, California 93940	1
5. Lt. Chaiyuth Tantrakul Royal Thai Navy 98/9 soi Intamara 10, Sudhisarn Rd., Bangkok, Thailand	2

Thesis 171278
T1374 Tantrakul
Th c.1 Condensation heat
Tl - transfer inside rotat-
c. ing heat pipes.
7 FEB 80 26219
24 JUN 82 28590
14 NOV 83 27863

Thesis 171278
T1374 Tantrakul
c.1 Condensation heat
transfer inside rotat-
ing heat pipes.

thesT1374

Condensation heat transfer inside rotati



3 2768 002 05460 3
DUDLEY KNOX LIBRARY